

Calculation of Incompressible Viscous Flows by an Unconditionally Stable Projection FEM

J.-L. Guermond* and L. Quartapelle†

*Laboratoire d'Informatique pour la Mécanique et les Sciences de l'Ingénieur, CNRS, BP 133, 91403, Orsay, France;

†Dipartimento di Fisica, Politecnico di Milano, Piazza Leonardo da Vinci, 32, 20133 Milano, Italy

E-mail: guermond@limsi.fr

Received December 4, 1995; revised June 10, 1996

This paper investigates the numerical performance of a finite element implementation of a new incremental fractional-step method to compute steady and unsteady incompressible viscous flows under general boundary conditions and using unstructured meshes. A variational framework is adopted which accommodates two different spaces for representing and approximating the velocity fields calculated respectively in the viscous and inviscid phases of the method, but which leads to a very simple numerical scheme in terms of only one discrete velocity field. An unconditionally stable semi-implicit approximation of the nonlinear term is used to eliminate any time-step restriction, as far as the numerical stability is concerned. Numerical results for five test problems in two dimensions are reported to illustrate the flexibility of the proposed method. © 1997 Academic Press

1. INTRODUCTION

The Chorin [4, 5] Temam [30, 29] fractional-step projection method is by far the most employed method for integrating the incompressible Navier–Stokes equations, especially in the finite element field (see, e.g., Donea *et al.* [7] and Gresho and Chan [12]). Despite that, a rigorous analysis for this kind of methods, with the effect of both temporal and spatial discretizations taken into account, has been attempted only recently (Guermond [13, 14]; see also [16, 17]).

An important feature of fractional-step projection methods is the structural difference existing between the equations of the viscous step and those of the incompressible phase of the calculation. In fact the first half-step constitutes an elliptic boundary value problem for an intermediate velocity unknown, accounting for the viscous diffusion and convection mechanisms, whereas the second half-step represents an essentially inviscid problem which determines the end-of-step divergence-free velocity field, together with a suitable approximation to the pressure distribution. In particular, boundary conditions of a different kind have to be imposed on the velocity fields which are calculated in each of the two half-steps.

Despite that, most (if not all) actual implementations of the projection method assume implicitly one and the same discrete representation for the two aforementioned velocity fields. But a single discretization cannot afford the best approximation of velocity simultaneously for both the viscous and inviscid phases of the method. Insufficient consideration of this difference lies at the origin of the difficulties which the practical implementation of fractional-step projection methods is still encountering at present.

The functional analytic setting which properly accounts for the different character of the equations of the two half-steps [13, 14] allows us to devise alternative formulations and spatial discretizations of the fractional-step method and to study their convergence and stability properties. In particular, a very simple projection method, based on a Poisson equation for pressure increment and eliminating the end-of-step velocity from the numerical scheme was proposed in [13, 14] as the most direct technique for simulating incompressible viscous flows in two- and three-dimensional regions of arbitrary shape under quite general boundary conditions. The aim of this article is to give a brief description of such a method and to report on the numerical performances of a 2D finite element implementation of it.

The content of the paper is organized as follows. Section 2 introduces the unsteady Navier–Stokes problem supplemented with various kinds of boundary conditions comprising the specification of tangential components of vorticity and the imposition of boundary values on pressure. In Section 3 the Navier–Stokes problem is formulated in a variational form after recalling the standard functional tools needed to analyze constrained parabolic problems. In particular, a semi-implicit approximation of the nonlinear convection term is considered. Section 4 introduces the additional functional analytic tools required to formulate the fractional-step projection method in variational form and describes an incremental version of the projection method. In Section 5 the issue of the spatial discretization is discussed. A numerical realization of the equations enforcing the incompressibility (the projection step) is consid-

ered which relies on a Poisson problem for the pressure (increment). The main result of this section consists in the algorithm (5.10)–(5.12) that should be implemented in practice. Section 6 describes the implementation of the proposed method by finite elements using a parabolic interpolation for velocity and a linear interpolation for pressure. The numerical tools employed for generating unstructured Delaunay triangulations and for solving the linear systems of finite element equations are indicated. The accuracy of the method in two dimensions is illustrated by some convergence tests. Finally, in Section 7 we illustrate the flexibility of the method on five examples: the square cavity, a triangular cavity, the steady flow past a backward-facing step, the unsteady flow past a NACA0012 airfoil at large incidence with massive separation, and finally, the unsteady flow past a multibody airfoil with slat and flap in landing configuration. The last section is devoted to some concluding remarks.

2. THE UNSTEADY NAVIER–STOKES PROBLEM

We want to illustrate the ability of the fractional-step projection method to accommodate various kinds of boundary conditions for flows in connected bounded domains Ω of \mathbb{R}^d ($d = 2$ or 3) with a conveniently smooth boundary $\partial\Omega$. In particular we will consider the imposition of derivative conditions on velocity and the enforcement of prescribed boundary values on pressure and introduce, accordingly, the following unsteady Navier–Stokes problem: For a given body force \mathbf{f} (possibly dependent on time) and a prescribed divergence-free initial velocity field \mathbf{u}_0 , find a velocity field \mathbf{u} and a pressure field p (per unit density) so that at $t = 0$, $\mathbf{u} = \mathbf{u}_0$, and at all subsequent times,

$$\mathcal{P} \begin{cases} \frac{\partial \mathbf{u}}{\partial t} - \nu \nabla^2 \mathbf{u} + (\mathbf{u} \cdot \nabla) \mathbf{u} + \nabla p = \mathbf{f}, \\ \nabla \cdot \mathbf{u} = 0, \end{cases} \quad (2.1)$$

the velocity and the pressure are subject to the following boundary conditions:

$$\begin{aligned} \mathbf{u}|_{\partial\Omega_1} &= \mathbf{b}_1; \\ \mathbf{u} \cdot \mathbf{n}|_{\partial\Omega_2} &= \mathbf{b}_2 \cdot \mathbf{n}, \quad (\alpha \mathbf{n} \times \mathbf{u} + \nabla \times \mathbf{u}) \times \mathbf{n}|_{\partial\Omega_2} = 0; \\ \mathbf{u} \times \mathbf{n}|_{\partial\Omega_3} &= \mathbf{b}_3 \times \mathbf{n}, \quad p|_{\partial\Omega_3} = c_3; \end{aligned} \quad (2.2)$$

where $\partial\Omega_1, \partial\Omega_2, \partial\Omega_3$ is a partition of $\partial\Omega$. The functions \mathbf{b}_i , $i = 1, 2, 3$, c_3 , and $\alpha \geq 0$ may depend on time and are assumed to be suitably smooth on the respective domain of definition, which is one of the parts of $\partial\Omega$. Moreover, the initial and boundary data are assumed to satisfy the compatibility condition [15; 23, p. 3]

$$\mathbf{u}_0 \cdot \mathbf{n}|_{\partial\Omega_{1,2}} = \mathbf{b}_{1,2} \cdot \mathbf{n}|_{t=0}. \quad (2.3)$$

The pressure boundary condition could be specified also in the more proper form $(p - \nabla \cdot \mathbf{u})|_{\partial\Omega_3} = c_3$, which is equivalent to the simpler form in (2.2) by virtue of the incompressibility condition. The boundary conditions involving the normal or tangential components of \mathbf{u} couple the vector components of the velocity field when the boundaries $\partial\Omega_2$ and $\partial\Omega_3$ are curved or are flat but oblique with respect to the Cartesian axes. The equations for the velocity components uncouple even in the presence of boundary conditions for \mathbf{u} different from purely Dirichlet ones, provided that the corresponding boundaries are parallel to the Cartesian planes. Note that a nonhomogeneous term can be included without difficulty in the derivative boundary condition of Robin type for velocity and that other types of boundary conditions could be easily accounted for, provided that the bilinear form associated with the Laplace operator is modified accordingly (see below). The last two boundary conditions in (2.2) are intended to mimic, more or less, conditions at outflow boundaries.

3. THE VARIATIONAL FORMULATION

To recast the unsteady problem \mathcal{P} in a variational form, we introduce the relevant Hilbert spaces. As usual, $L^2(\Omega)$ denotes the space of real-valued functions, the squares of which are square summable in Ω . We denote the inner product in $L^2(\Omega)$ by (\cdot, \cdot) and its norm by $|\cdot|_0$. $H^m(\Omega)$, $m \geq 0$, is the space of functions the derivatives of which, up to order m , are square summable functions. The space $H^m(\Omega)$, equipped with the norm $\|u\|_m^2 = (\sum_{|\alpha|=0}^m |D^\alpha u|_0^2)^{1/2}$, expressed in the multi-index notation, is a Hilbert space.

Furthermore, we introduce

$$\mathbf{X}_0 = \{\mathbf{v} \in \mathbf{H}^1(\Omega) \mid \mathbf{v}|_{\partial\Omega_1} = 0, \mathbf{v} \cdot \mathbf{n}|_{\partial\Omega_2} = 0, \mathbf{v} \times \mathbf{n}|_{\partial\Omega_3} = 0\} \quad (3.1)$$

$$M = L^2(\Omega) \quad (3.2)$$

$$\mathbf{V}_0 = \{\mathbf{v} \in \mathbf{X}_0 \mid \nabla \cdot \mathbf{v} = 0\} \quad (3.3)$$

$$\mathbf{J}_0 = \{\mathbf{v} \in \mathbf{L}^2(\Omega) \mid \nabla \cdot \mathbf{v} = 0, \mathbf{v} \cdot \mathbf{n}|_{\partial\Omega_1 \cup \partial\Omega_2} = 0\}. \quad (3.4)$$

Denote by $H_{0,\partial\Omega_3}^1(\Omega)$ the space of scalar functions of $H^1(\Omega)$ the trace of which is zero on $\partial\Omega_3$. The importance of $\mathbf{J}_0 = \mathbf{J}_{0,\partial\Omega_{1,2}}(\Omega)$ and $H_{0,\partial\Omega_3}^1(\Omega)$ for the incompressible problem considered here is brought to light by the orthogonal decomposition of $L^2(\Omega)$,

$$L^2(\Omega) = \mathbf{J}_{0,\partial\Omega_{1,2}}(\Omega) \oplus \nabla(H_{0,\partial\Omega_3}^1(\Omega)) \quad (3.5)$$

which follows from the application of the divergence theorem. The discrete counterpart of this decomposition plays

a key role in the projection technique under the mixed boundary conditions considered here.

For the sake of simplicity, it is hereafter assumed that $\text{meas}(\partial\Omega_3) > 0$ so that the pressure is uniquely defined in M . If this hypothesis is not satisfied, we have to take the quotient of $L^2(\Omega)$ by constants, i.e., $M = L^2(\Omega)/\mathbb{R}$ (see [17] for other details).

A variational version of problem (2.1)–(2.2) reads: For f smooth enough in time with values in $L^2(\Omega)$ and \mathbf{u}_0 in $\mathbf{H}^2(\Omega)$ with $\nabla \cdot \mathbf{u}_0 = 0$ and $\mathbf{u}_0 \cdot \mathbf{n}|_{\partial\Omega_{1,2}} = \mathbf{b}_{1,2} \cdot \mathbf{n}|_{t=0}$, find a pair (\mathbf{u}, p) which is smooth in time so that

$$\begin{aligned} \mathbf{u}|_{t=0} &= \mathbf{u}_0, \\ \mathbf{u} &\in \mathbf{H}^1(\Omega), \\ p &\in M, \end{aligned} \quad \left\{ \begin{array}{l} \mathbf{u}|_{\partial\Omega_1} = \mathbf{b}_1, \\ \mathbf{u} \cdot \mathbf{n}|_{\partial\Omega_2} = \mathbf{b}_2 \cdot \mathbf{n}, \\ \mathbf{u} \times \mathbf{n}|_{\partial\Omega_3} = \mathbf{b}_3 \times \mathbf{n}, \end{array} \right. \quad (3.6)$$

and such that for all times $t > 0$

$$\begin{aligned} \left(\frac{\partial \mathbf{u}}{\partial t}, \mathbf{v} \right) + a(\mathbf{u}, \mathbf{v}) + b(\mathbf{u}, \mathbf{u}, \mathbf{v}) - (p, \nabla \cdot \mathbf{v}) \\ = (\mathbf{f}, \mathbf{v}) - \int_{\partial\Omega_3} c_3 \mathbf{v} \cdot \mathbf{n}, \quad \forall \mathbf{v} \in \mathbf{X}_0, \\ (\nabla \cdot \mathbf{u}, q) = 0, \quad \forall q \in M. \end{aligned} \quad (3.7)$$

Here, to simplify the momentum equation, we have introduced the following notations for the bilinear form,

$$\begin{aligned} a(\mathbf{u}, \mathbf{v}) &= \nu(\nabla \cdot \mathbf{u}, \nabla \cdot \mathbf{v}) + \nu(\nabla \times \mathbf{u}, \nabla \times \mathbf{v}) \\ &+ \nu \int_{\partial\Omega_2} \alpha(\mathbf{u} \times \mathbf{n}) \cdot (\mathbf{v} \times \mathbf{n}), \end{aligned} \quad (3.8)$$

and for the trilinear form

$$b(\mathbf{u}, \mathbf{v}, \mathbf{w}) = ((\mathbf{u} \cdot \nabla)\mathbf{v}, \mathbf{w}) + \frac{1}{2}(\nabla \cdot \mathbf{u}, \mathbf{v} \cdot \mathbf{w}). \quad (3.9)$$

Note that the trilinear form $b(\mathbf{u}, \mathbf{v}, \mathbf{w})$ corresponds to the usual advective term $(\mathbf{u} \cdot \nabla)\mathbf{v}$ when \mathbf{u} is divergence free.

The conditions on the trace, the normal trace, and the tangential trace of the velocity on $\partial\Omega_1$, $\partial\Omega_2$, and $\partial\Omega_3$, respectively, are all essential boundary conditions. The condition involving the tangential components of $\nabla \times \mathbf{u}$ on $\partial\Omega_2$ is a natural boundary condition of Robin type. The pressure boundary condition on $\partial\Omega_3$ is natural as well; actually, the weak formulation enforces the natural boundary condition $(p - \nabla \cdot \mathbf{u})|_{\partial\Omega_3} = c_3$, as already noticed.

It should be remarked that the use of the bilinear form $(\nabla \cdot \mathbf{u}, \nabla \cdot \mathbf{v}) + (\nabla \times \mathbf{u}, \nabla \times \mathbf{v})$ is mandatory when the boundaries $\partial\Omega_2$ and $\partial\Omega_3$, where the condition prescribed on velocity is not of a mere Dirichlet type, are curved. On the contrary, the more common bilinear form $(\nabla \mathbf{u}, \nabla \mathbf{v})$

can be used only when Dirichlet conditions are specified for \mathbf{u} or when the boundaries $\partial\Omega_2$ and $\partial\Omega_3$ are flat and parallel to the Cartesian axes. Note also that the coupling between the velocity components, engendered by the presence of mixed boundary conditions, appears in the definition of the test functions of \mathbf{X}_0 .

The conservative form of the nonlinear term defined in (3.9) is frequently considered along with the hypothesis $\text{meas}(\partial\Omega_3) = 0$. This form can be used also for channel or exterior flows with an ‘‘outflow’’ boundary, provided that the boundary in question is located downstream, far enough from any recirculatory zone, so that the condition $\mathbf{u} \cdot \mathbf{n}|_{\partial\Omega_3} \geq 0$ is assured. In practice this treatment of the nonlinear term can guarantee some ‘‘unconditional’’ stability to the numerical scheme [16]. More precisely, its spatially discretized counterpart does not contribute to the kinetic energy of the solution and boundedness of the kinetic energy is guaranteed by the viscous dissipation mechanisms.

It is assumed in the following that problem (3.6)–(3.7) has a unique solution and that this solution is as smooth as needed and that all of the possible compatibility conditions on the data required by the smoothness of the solution are satisfied; for a mathematical discussion of these hypotheses the reader is referred to Heywood and Rannacher [19].

4. THE FRACTIONAL-STEP ALGORITHM

The variational formulation (3.6)–(3.7) is adequate for approximating the Navier–Stokes equations by means of coupled solution methods. On the contrary, to build a fractional-step projection method additional tools are required since, as explained in the introduction, this kind of method implies a separate treatment of the viscous and incompressible parts of the problem. As a consequence, the appropriate functional setting for a fractional-step method must accommodate another functional space for representing the velocity field calculated in the incompressible inviscid step of the method [14], defined as

$$\mathbf{H}_0^{\text{div}} = \{\mathbf{v} \in \mathbf{L}^2(\Omega) \mid \nabla \cdot \mathbf{v} \in L^2(\Omega), \mathbf{v} \cdot \mathbf{n}|_{\partial\Omega_{1,2}} = 0\}. \quad (4.1)$$

To relate the two velocity spaces it is necessary to introduce the injection operator i from \mathbf{X}_0 to $\mathbf{H}_0^{\text{div}}$ and its transpose i^t from the dual space $(\mathbf{H}_0^{\text{div}})'$ to \mathbf{X}'_0 . On the other hand, two divergence operators must be introduced, one denoted to $\nabla \cdot$ which maps vector fields belonging to \mathbf{X}_0 onto scalar functions of M and the other denoted by $\hat{\nabla} \cdot$ which is the extension of the latter to the vector space $\mathbf{H}_0^{\text{div}}$. The respective transpose operators are denoted by $(\nabla \cdot)^t$ and $(\hat{\nabla} \cdot)^t$; note that $(\nabla \cdot)^t \neq -\nabla$ since $(\nabla \cdot)^t p = -\nabla p$ only if $p \in H_{0,\partial\Omega_3}^1(\Omega)$. The relationship between the opera-

tors and the spaces is depicted by the following commutative diagram:

$$\begin{array}{ccc}
 \mathbf{X}_0 & \xrightarrow{\nabla \cdot} & M \\
 \downarrow i & \nearrow \hat{\nabla} \cdot & \\
 \mathbf{H}_0^{\text{div}} & &
 \end{array}$$

Even though, in the continuous case the difference between the spaces \mathbf{X}_0 and $\mathbf{H}_0^{\text{div}}$ may seem subtle (or even pedantically unwitty), in the spatially discrete case such a distinction is important since it implies two different discrete counterparts of the divergence operator, and also of its transpose the gradient operator.

The fractional-step method is formulated by introducing a partition of the time interval $[0, T]$: $t^k = k \delta t$ for $0 \leq k \leq K$, where $\delta t = T/K$. To avoid the technical difficulty of the possible blowup of the estimates at the initial time induced by the possible lack of regularity of the continuous solution, we suppose that the solution has a suitable regularity in time as $t \rightarrow 0$.

To circumvent the (theoretical) difficulty due to the presence of the nonhomogeneous boundary condition on pressure, we assume that we have at hand a smooth pressure lifting $P(t)$ so that $P(t)|_{\partial\Omega_3} = c_3(t)$. Hereafter (up to further notice), we make the change of variable

$$\pi(t) = p(t) - P(t),$$

which implies to enforce the natural boundary condition $\pi(t)|_{\partial\Omega_3} = 0$.

Now we discretize the problem in time by means of a semi-implicit first-order accurate Euler scheme in which the advection term is linearized in the conservative form (3.9). The weak formulation of the fractional-step method in incremental form reads as follows. We assume that $\mathbf{u}_0 \in H^2(\Omega)$, with $\nabla \cdot \mathbf{u}_0 = 0$; then we set $\mathbf{u}^0 = \mathbf{u}_0$. Furthermore, we assume that we have at hand $\pi(t=0)$ and that $\pi(0) \in H^1(\Omega)$; then we set $\pi^0 = \pi(0)$. Then, we define two sequences of approximate velocities $\{\mathbf{u}^k \in \mathbf{X}_{b^k}\}$ and $\{\hat{\mathbf{u}}^k \in \mathbf{H}_{b^k, \mathbf{n}}^{\text{div}}\}$ ¹ and one sequence of approximate pressure $\{\pi^k \in M\}$, $k \geq 1$, calculated in two successive separate steps, the former accounting for the viscosity effect and the latter to enforce incompressibility and evaluate the pressure field.

The viscous step consists in, for $k \geq 0$ and $\mathbf{f}^{k+1} \in L^2(\Omega)$, finding an intermediate velocity field

$$\mathbf{u}^{k+1} \in \mathbf{H}^1(\Omega), \quad \begin{cases} \mathbf{u}|_{\partial\Omega_1}^{k+1} = \mathbf{b}_1^{k+1}, \\ \mathbf{u}^{k+1} \cdot \mathbf{n}|_{\partial\Omega_2} = \mathbf{b}_2^{k+1} \cdot \mathbf{n}, \\ \mathbf{u}^{k+1} \times \mathbf{n}|_{\partial\Omega_3} = \mathbf{b}_3^{k+1} \times \mathbf{n}, \end{cases} \quad (4.2)$$

such that

$$\begin{aligned} & \left(\frac{\mathbf{u}^{k+1} - i^t \hat{\mathbf{u}}^k}{\delta t}, \mathbf{v} \right) + a(\mathbf{u}^{k+1}, \mathbf{v}) + b(\mathbf{u}^k, \mathbf{u}^{k+1}, \mathbf{v}) \\ & = (\mathbf{f}^{k+1}, \mathbf{v}) + (\pi^k, \nabla \cdot \mathbf{v}) - (\nabla P^{k+1}, \mathbf{v}), \quad \forall \mathbf{v} \in \mathbf{X}_0. \end{aligned} \quad (4.3)$$

The use of the symbol \mathbf{u}^{k+1} to indicate the *intermediate* velocity is unusual; but the advantage of adopting such a notation will become evident in the following.

The incompressible (projection) step of the method consists in finding a pair $(\hat{\mathbf{u}}^{k+1}, \pi^{k+1})$ with

$$\begin{aligned} \hat{\mathbf{u}}^{k+1} & \in \mathbf{H}^{\text{div}}, \quad \hat{\mathbf{u}}^{k+1} \cdot \mathbf{n}|_{\partial\Omega_{1,2}} = \mathbf{b}_{1,2}^{k+1} \cdot \mathbf{n}, \\ \pi^{k+1} & \in M, \end{aligned} \quad (4.4)$$

where $\mathbf{H}^{\text{div}} = \{\mathbf{v} \in L^2(\Omega) \mid \nabla \cdot \mathbf{v} \in L^2(\Omega)\}$ and such that

$$\begin{aligned} & \left(\frac{\hat{\mathbf{u}}^{k+1} - i \mathbf{u}^{k+1}}{\delta t}, \hat{\mathbf{v}} \right) - ((\pi^{k+1} - \pi^k), \hat{\nabla} \cdot \hat{\mathbf{v}}) = 0, \quad \forall \hat{\mathbf{v}} \in \mathbf{H}_0^{\text{div}}, \\ & (\hat{\nabla} \cdot \hat{\mathbf{u}}^{k+1}, q) = 0, \quad \forall q \in M. \end{aligned} \quad (4.5)$$

5. SPATIAL DISCRETIZATION

5.1. The Discrete Setting

We now consider the spatial discretization of a fractional-step method, by introducing finite-dimensional spaces for approximating the velocity fields \mathbf{u} and $\hat{\mathbf{u}}$ and the pressure field p involved in the viscous and inviscid steps of the method.

Let $\mathbf{X}_{0,h}$ be a finite-dimensional subspace of \mathbf{X}_0 . We endow $\mathbf{X}_{0,h}$ with the norm of $\mathbf{H}^1(\Omega)$. Furthermore, we introduce $\mathbf{X}'_{0,h}$ and the dual space of $\mathbf{X}_{0,h}$ ($\mathbf{X}_{0,h}$ and $\mathbf{X}'_{0,h}$ are identical in terms of vector spaces but their norms are different). Likewise, we define M_h a finite dimensional subspace of M that we endow with the norm of $L^2(\Omega)$.

We assume that $\mathbf{X}_{0,h}$ and M_h are internal approximations of \mathbf{X}_0 and M in the sense that they satisfy the following properties (see, e.g., Bernardi and Raugel [1], Girault and Raviart [11], or Quarteroni and Valli [24] for other details). There is some $\ell \geq 1$ such that, for all $\mathbf{v} \in \mathbf{H}^{\ell+1}(\Omega) \cap \mathbf{X}_0$

¹ \mathbf{X}_{b^k} is a shorthand for $\mathbf{X}_{b_1, b_2, n, b_3 \times n}$ whilst $\mathbf{H}_{b^k, \mathbf{n}}^{\text{div}}$ is a shorthand for $\mathbf{H}_{b_1, b_2, \mathbf{n}}^{\text{div}}$.

and for all $q \in H^\ell(\Omega) \cap M$, there are approximations $r_h \mathbf{v} \in \mathbf{X}_{0,h}$ and $\rho_h q \in M_h$ such that

$$|\mathbf{v} - r_h \mathbf{v}|_0 + h|\mathbf{v} - r_h \mathbf{v}|_1 \leq ch^{\ell+1}|\mathbf{v}|_{\ell+1}, \quad |q - \rho_h q|_0 \leq ch^\ell|q|_\ell,$$

where ℓ represents, roughly speaking, the degree of the polynomial interpolation of velocity (more precisely, in case of finite element interpolation, ℓ is the degree of interpolation of the velocity, and the degree of interpolation of the pressure, ℓ' , is assumed to satisfy $0 \leq \ell - 1 \leq \ell' \leq \ell$; see below).

We introduce now a discrete version of the divergence operator: $\nabla_h \cdot : \mathbf{X}_{0,h} \rightarrow M_h$ so that for all $\mathbf{v}_h \in \mathbf{X}_{0,h}$ and $q_h \in M_h$, $(\nabla_h \cdot \mathbf{v}_h, q_h) = (\nabla \cdot \mathbf{v}_h, q_h)$. The stability and convergence analysis of the scheme to be presented below requires that $\nabla_h \cdot$ is surjective (cf. [17]); that is, $\mathbf{X}_{0,h}$ and M_h are compatible in the sense that they satisfy the inf-sup condition [2]

$$\exists \beta > 0, \quad \inf_{q_h \in M_h} \sup_{\mathbf{v}_h \in \mathbf{X}_{0,h}} (\nabla_h \cdot \mathbf{v}_h, q_h) \geq \beta |\mathbf{v}_h|_1 |q_h|_0. \quad (5.1)$$

It must be remarked that the approximate method to be described hereafter is not restricted to finite element interpolations, but it can accommodate any kind of spatial interpolation method which is compatible with the variational framework, such as, e.g., spectral interpolations P_N/P_{N-2} .

Passing to the approximation of the inviscid projection step, we define $\hat{\mathbf{X}}_{0,h}$ to be a finite-dimensional subspace of $L^2(\Omega)$ and endow $\hat{\mathbf{X}}_{0,h}$ with the norm of $L^2(\Omega)$; for the sake of simplicity we assume that $\mathbf{X}_{0,h} \subset \hat{\mathbf{X}}_{0,h}$ (in terms of vector space) and we denote by i_h the continuous injection of $\mathbf{X}_{0,h}$ into $\hat{\mathbf{X}}_{0,h}$; the transpose of i_h is the L^2 projection of $\hat{\mathbf{X}}_{0,h}$ onto $\mathbf{X}_{0,h}$. Note that $\hat{\mathbf{X}}_{0,h}$ is an internal approximation of $L^2(\Omega)$ for $\mathbf{X}_{0,h}$ is an approximation of \mathbf{X}_0 and \mathbf{X}_0 is dense in $L^2(\Omega)$. Furthermore, we assume that $\hat{\mathbf{X}}_{0,h}$ and M_h are compatible in the sense that

- either $\hat{\mathbf{X}}_{0,h}$ is conformal in

$$\mathbf{H}_0^{\text{div}} = \{\mathbf{v} \in L^2(\Omega) \mid \nabla \cdot \mathbf{v} \in L^2(\Omega), \mathbf{v} \cdot \mathbf{n}|_{\partial\Omega_{1,2}} = 0\}$$

- or M_h is conformal in $H_{0,\partial\Omega_3}^1(\Omega)$.

For instance, a possible choice is $\hat{\mathbf{X}}_{0,h} = \mathbf{X}_{0,h}$, but we can also choose $\hat{\mathbf{X}}_{0,h} \subset \mathbf{H}_0^{\text{div}}$; in the following we will concentrate on the choice $\hat{\mathbf{X}}_{0,h} \subset L^2(\Omega)$ and $M_h \subset H_{0,\partial\Omega_3}^1(\Omega)$ (see [14] for other details).

The analysis of the fractional-step equations in spatially discrete form requires us to introduce another discrete

version of the operator $\nabla \cdot$. We define $\hat{\nabla}_h \cdot : \hat{\mathbf{X}}_{0,h} \rightarrow M_h$ so that for every couple $(\hat{\mathbf{v}}, q)$ in $\hat{\mathbf{X}}_{0,h} \times M_h$ we have either

- $(\hat{\nabla}_h \cdot \hat{\mathbf{v}}, q) = (\nabla \cdot \hat{\mathbf{v}}, q)$ if $\hat{\mathbf{X}}_{0,h} \subset \mathbf{H}_0^{\text{div}}$ or
- $(\hat{\nabla}_h \cdot \hat{\mathbf{v}}, q) = -(\hat{\mathbf{v}}, \hat{\nabla}_h q)$ if $M_h \subset H_{0,\partial\Omega_3}^1(\Omega)$.

Of course this definition makes sense thanks to the compatibility we require between $\hat{\mathbf{X}}_{0,h}$ and M_h . The relation between $\nabla_h \cdot$ and $\hat{\nabla}_h \cdot$ is such that $\hat{\nabla}_h \cdot$ is an extension of $\nabla_h \cdot$ and $i_h^t \hat{\nabla}_h = \nabla_h$, where we have set $\nabla_h = -(\nabla_h \cdot)^t$ and $\hat{\nabla}_h = -(\hat{\nabla}_h \cdot)^t$; in other words we have the following commutative diagram:

$$\begin{array}{ccc} \mathbf{X}_{0,h} & \xrightarrow{\nabla_h \cdot} & M_h \\ \downarrow i_h & \nearrow \hat{\nabla}_h \cdot & \\ \hat{\mathbf{X}}_{0,h} & & \end{array}$$

Note that $\hat{\nabla}_h \cdot$ is surjective since $\hat{\nabla}_h \cdot$ is an extension of $\nabla_h \cdot$.

The null space of $\hat{\nabla}_h \cdot$ playing an important role in the spatially discrete projection method, we define

$$\hat{\mathbf{J}}_{0,h} = \ker(\hat{\nabla}_h \cdot). \quad (5.2)$$

The definitions above enable us to build a discrete counterpart of the aforementioned orthogonal decomposition $L^2(\Omega) = \mathbf{J}_{0,\partial\Omega_{1,2}}(\Omega) \oplus \nabla(H_{0,\partial\Omega_3}^1(\Omega))$, which reads

$$\hat{\mathbf{X}}_{0,h} = \hat{\mathbf{J}}_{0,h} \oplus \hat{\nabla}_h(M_h). \quad (5.3)$$

We are now finally able to define the spatially discrete version of the incremental fractional-step method. Define two sequences of approximate velocities $\{\mathbf{u}_h^k \in \mathbf{X}_{b^k,n,h}\}$ and $\{\hat{\mathbf{u}}_h^k \in \hat{\mathbf{X}}_{b^k,n,h}\}$ and one sequence of approximate pressures $\{\pi_h^k \in M_h\}$ as follows. The viscous step reads: find $\mathbf{u}_h^{k+1} \in \mathbf{X}_{b^{k+1},h}$,

$$\begin{aligned} & \left(\frac{\mathbf{u}_h^{k+1} - i_h \hat{\mathbf{u}}_h^k}{\delta t}, \mathbf{v}_h \right) + a(\mathbf{u}_h^{k+1}, \mathbf{v}_h) + b(\mathbf{u}_h^k, \mathbf{u}_h^{k+1}, \mathbf{v}_h) \\ & = (\mathbf{f}^{k+1}, \mathbf{v}_h) + (\pi_h^k, \nabla \cdot \mathbf{v}_h) - (\nabla P^{k+1}, \mathbf{v}_h), \quad \forall \mathbf{v}_h \in \mathbf{X}_{0,h}. \end{aligned} \quad (5.4)$$

The incompressible (projection) step of the method consists in finding $\hat{\mathbf{u}}_h^{k+1} \in \hat{\mathbf{X}}_{b^{k+1},n,h}$ and $\pi_h^{k+1} \in M_h$ such that

$$\begin{aligned} & \left(\frac{\hat{\mathbf{u}}_h^{k+1} - i_h \mathbf{u}_h^{k+1}}{\delta t}, \hat{\mathbf{v}}_h \right) - ((\pi_h^{k+1} - \pi_h^k), \hat{\nabla}_h \cdot \hat{\mathbf{v}}_h) = 0, \quad \forall \hat{\mathbf{v}}_h \in \hat{\mathbf{X}}_{0,h}, \\ & (\hat{\nabla}_h \cdot \hat{\mathbf{u}}_h^{k+1}, q_h) = 0, \quad \forall q_h \in M_h. \end{aligned} \quad (5.5)$$

Remark. Problem (5.5) is well posed since $\hat{\nabla}_h \cdot$ is surjective. The pair

$$\hat{\mathbf{u}}_h^{k+1} \text{ and } \delta t \hat{\nabla}_h(\pi_h^{k+1} - \pi_h^k)$$

represents the decomposition of the *injected* intermediate velocity $i_h \mathbf{u}_h^{k+1}$ in $\hat{\mathbf{J}}_{0,h} \oplus \hat{\nabla}_h(M_h)$; in other words, $\hat{\mathbf{u}}_h^{k+1} = \mathbb{P}_{\hat{\mathbf{J}}_{0,h}}(i_h \mathbf{u}_h^{k+1})$, where $\mathbb{P}_{\hat{\mathbf{J}}_{0,h}}$ is the operator of orthogonal projection of $\hat{\mathbf{X}}_{0,h}$ onto $\hat{\mathbf{J}}_{0,h}$.

5.2. The Projection Step as a Poisson Problem

We now choose M_h as an internal approximation of $H_{0,\partial\Omega_3}^1(\Omega)$ (recall that in the previous sections we only required $M_h \subset L^2(\Omega)$) and denote it by $N_{0,h}$, to make this distinction explicit. We also choose

$$\hat{\mathbf{X}}_{0,h} = \mathbf{X}_{0,h} + \nabla N_{0,h}. \quad (5.6)$$

Note that this definition makes sense for, $N_{0,h}$ being a subspace of $H_{0,\partial\Omega_3}^1(\Omega)$, $\nabla N_{0,h}$ is in $L^2(\Omega)$, that is to say, $\hat{\mathbf{X}}_{0,h}$ is a subspace of $L^2(\Omega)$ as required by the theory developed in [17]. We also define N_h the finite element space composed of the degrees of freedom of $N_{0,h}$ plus those living on $\partial\Omega_3$.

In this framework the viscous step amounts to looking for \mathbf{u}_h^{k+1} in $\mathbf{X}_{b^{k+1},h}$ so that we have

$$\begin{aligned} & \left(\frac{\mathbf{u}_h^{k+1} - i_h^1 \hat{\mathbf{u}}_h^k}{\delta t}, \mathbf{v}_h \right) + a(\mathbf{u}_h^{k+1}, \mathbf{v}_h) + b(\mathbf{u}_h^k, \mathbf{u}_h^{k+1}, \mathbf{v}_h) \\ & = (\mathbf{f}^{k+1}, \mathbf{v}_h) - (\nabla \pi_h^k, \mathbf{v}_h) - (\nabla P_h^{k+1}, \mathbf{v}_h) \quad \forall \mathbf{v}_h \in \mathbf{X}_{0,h}, \end{aligned} \quad (5.7)$$

where P_h^{k+1} is some good approximation of $P(t^{k+1})$. Thanks to the choice $N_{0,h} \subset H_{0,\partial\Omega_3}^1(\Omega)$, we can prove that $\hat{\nabla}_h$ is the restriction of ∇ to $N_{0,h}$ (in the distributional sense). As a result the projection step can be formulated as follows: find π_h^{k+1} in $N_{0,h}$ so that

$$(\nabla(\pi_h^{k+1} - \pi_h^k), \nabla q_h) = - \frac{(\nabla \cdot \mathbf{u}_h^{k+1}, q_h)}{\delta t} \quad \forall q_h \in N_{0,h}, \quad (5.8)$$

and then set (in terms of distributions)

$$\hat{\mathbf{u}}_h^{k+1} = \mathbf{u}_h^{k+1} - \delta t \nabla(\pi_h^{k+1} - \pi_h^k). \quad (5.9)$$

Therefore, the projection step amounts to solving a discrete Poisson equation with a homogeneous Neumann condition on $\partial\Omega_1 \cup \partial\Omega_2$ and a Dirichlet boundary condition on $\partial\Omega_3$; cf. also Rannacher [25].

Note that, as a consequence of the time-stepping of a fractional kind, the boundary condition $(p - \nabla \cdot \mathbf{u})_{\partial\Omega_3} = c_3$ is enforced through *two separate* conditions: the natural condition $\nabla \cdot \mathbf{u}_{\partial\Omega_3}^{k+1} = 0$ accounted for in the weak equation

(5.7) and the condition $p_h^{k+1}|_{\partial\Omega_3} = c_{3,h}^{k+1}$ which is satisfied thanks to the chosen lifting and the Dirichlet condition $\pi_h^{k+1}|_{\partial\Omega_3} = 0$ in Poisson problem (5.8).

5.3. Algorithm with the End-of-Step Velocity Eliminated

In practice it is not convenient to use Eq. (5.7) directly, since it contains the end-of-step velocity $\hat{\mathbf{u}}_h^k$ which belongs to a space different from that of the intermediate velocity \mathbf{u}_h^{k+1} , and it contains a lifting $P(t)$ which is somewhat arbitrary. The purpose of this section is to show that the end-of-step velocity and the pressure lifting can be eliminated.

Since the pressure lifting is arbitrary, for $k \geq 0$, we define $P_h^{k+1} \in N_h$ so that $P_h^{k+1}|_{\partial\Omega_3} = c_{3,h}^{k+1}$ and

$$(\nabla P_h^{k+1}, \nabla q_h) = 0 \quad \forall q_h \in N_{0,h}.$$

The algorithm is initialized by setting $\mathbf{u}_h^0 = \mathbf{u}_{0,h}$, where $\mathbf{u}_{0,h}$ is an approximation of the initial data \mathbf{u}_0 in $\mathbf{X}_{b(0),h}$. Then we suppose that an approximate initial pressure p_h^0 is available or can be calculated by means of some first-order algorithm. There are numerous choices to do this, but the way of calculating this approximation is not important, provided it is first-order accurate in time and space.

For $k \geq 1$, the end-of-step velocity $\hat{\mathbf{u}}_h^k$ can be eliminated from the intermediate step. Indeed, for $k \geq 1$ we have (recall that $i_h^1 \hat{\nabla}_h = \nabla_h$)

$$i_h^1 \hat{\mathbf{u}}_h^k = \mathbf{u}_h^k - \delta t \nabla_h(\pi_h^k - \pi_h^{k-1}).$$

As a result, for $k \geq 1$, the intermediate step reads: find a velocity field $\mathbf{u}_h^{k+1} \in \mathbf{X}_{b^{k+1},h}$ such that

$$\begin{aligned} & \left(\frac{\mathbf{u}_h^{k+1} - \mathbf{u}_h^k}{\delta t}, \mathbf{v}_h \right) + a(\mathbf{u}_h^{k+1}, \mathbf{v}_h) + b(\mathbf{u}_h^k, \mathbf{u}_h^{k+1}, \mathbf{v}_h) \\ & = (\mathbf{f}^{k+1}, \mathbf{v}_h) - (\nabla(2\pi_h^k - \pi_h^{k-1}), \mathbf{v}_h) - (\nabla P_h^{k+1}, \mathbf{v}_h). \end{aligned}$$

The pressure lifting can be eliminated from this equation if we replace P_h^{k+1} by $2P_h^k - P_h^{k-1}$; this change of source term introduces an error of order δt^2 , but it *does not affect* the stability of the algorithm for we modify only a *source term*. The intermediate step takes the final form: for $k = 0$, we look for $\mathbf{u}_h^1 \in \mathbf{X}_{b^1,h}$ such that, for all $\mathbf{v}_h \in \mathbf{X}_{0,h}$,

$$\begin{aligned} & \left(\frac{\mathbf{u}_h^1 - \mathbf{u}_h^0}{\delta t}, \mathbf{v}_h \right) + a(\mathbf{u}_h^1, \mathbf{v}_h) + b(\mathbf{u}_h^0, \mathbf{u}_h^1, \mathbf{v}_h) \\ & = (\mathbf{f}^1, \mathbf{v}_h) - (\nabla p_h^0, \mathbf{v}_h). \end{aligned} \quad (5.10)$$

For $k \geq 1$, find a $\mathbf{u}_h^{k+1} \in \mathbf{X}_{b^{k+1},h}$ such that, for all $\mathbf{v}_h \in \mathbf{X}_{0,h}$,

$$\begin{aligned} & \left(\frac{\mathbf{u}_h^{k+1} - \mathbf{u}_h^k}{\delta t}, \mathbf{v}_h \right) + a(\mathbf{u}_h^{k+1}, \mathbf{v}_h) + b(\mathbf{u}_h^k, \mathbf{u}_h^{k+1}, \mathbf{v}_h) \\ & = (\mathbf{f}^{k+1}, \mathbf{v}_h) - (\nabla(2p_h^k - p_h^{k-1}), \mathbf{v}_h). \end{aligned} \quad (5.11)$$

For $k \geq 0$, the projection step reads: find $\pi_h^{k+1} \in N_{0,h}$ such that, for all $q_h \in N_{0,h}$,

$$(\nabla(\pi_h^{k+1} - \pi_h^k), \nabla q_h) = - \frac{(\nabla \cdot \mathbf{u}_h^{k+1}, q_h)}{\delta t}.$$

Thanks to the particular choice we have made for the pressure lifting, the projection step can be equivalently written in the (final) form: for $k \geq 0$, find $p_h^{k+1} \in N_{c_{3,h}^{k+1},h}$ such that, for all $q_h \in N_{0,h}$,

$$(\nabla(p_h^{k+1} - p_h^k), \nabla q_h) = - \frac{(\nabla \cdot \mathbf{u}_h^{k+1}, q_h)}{\delta t}. \quad (5.12)$$

Hence, the pressure lifting is eliminated from the algorithm that is implemented in practice: (5.10)–(5.12).

Remark. Note that, since the end-of-step velocity does not appear any more in the algorithm, the weird velocity space $\hat{\mathbf{X}}_{0,h}$ is completely eliminated from practical calculations.

The description of the proposed incremental fractional-step projection method is concluded by reminding the following result established in [17].

THEOREM. *Under convenient regularity assumptions on the data \mathbf{f} , \mathbf{u}_0 , \mathbf{b} , and if δt is small enough, the solution to the incremental projection scheme (5.10)–(5.12) satisfies the error bounds:*

$$\max_{0 \leq k \leq K} |\mathbf{u}(t^k) - \mathbf{u}_h^k|_0 + \max_{0 \leq k \leq K} |\mathbf{u}(t^k) - \hat{\mathbf{u}}_h^k|_0 \leq c[\mathbf{u}, p](\delta t + h^{\ell+1}),$$

$$\begin{aligned} & \left[\delta t \sum_{k=0}^K |\mathbf{u}(t^k) - \mathbf{u}_h^k|_1^2 \right]^{1/2} + \left[\delta t \sum_{k=1}^K |p(t^k) - p_h^k|_0^2 \right]^{1/2} \\ & \leq c[\mathbf{u}, p](\delta t + h^\ell), \end{aligned}$$

where ℓ is the interpolation degree of the velocity.

6. FINITE ELEMENT IMPLEMENTATION

6.1. Finite Element Equations

To construct a finite-element-based approximation of the projection method it is necessary to find a pair of polynomial representations for the velocity and pressure which satisfies the inf-sup condition (5.1). Finite elements satisfying this condition are well known: the most natural

interpolation is (P_2/P_1) for which $\ell = 2$ and it will be considered in the following; other possible interpolations are $(P_1 \text{ bubble}/P_1)$ or $(P_1 \text{ iso } P_2/P_1)$, for which $\ell = 1$ (cf. Girault and Raviart [11] for a review on this issue).

Coming to the approximation of the viscous step (5.11) (as well as (5.10)), we note that the conservative form of the nonlinear term defined in (3.9) leaves the Cartesian components of the velocity unknown \mathbf{u}_h^{k+1} uncoupled, as far as the advection term is concerned. Thus, we can introduce a ‘‘scalar’’ counterpart of the trilinear form $b(\mathbf{u}, \mathbf{v}, \mathbf{w})$ as

$$b_s(\mathbf{u}, v, w) = ((\mathbf{u} \cdot \nabla)v, w) + \frac{1}{2}(\nabla \cdot \mathbf{u}, vw).$$

On the other hand, the bilinear form $a(\mathbf{u}, \mathbf{v})$ of the viscous term in the momentum equation does couple the vector components of \mathbf{u} , except when Dirichlet conditions for velocity are prescribed on the entire boundary and in other particular circumstances. In these cases, the general bilinear form (3.8) can be replaced by the standard bilinear form for a scalar equation

$$a_s(u, v) = \nu(\nabla u, \nabla v).$$

When a complete velocity uncoupling is possible, each Cartesian component $u_{i,h}^{k+1}$, $i = 1, \dots, d$, of the intermediate velocity can be obtained by solving the *scalar* problem:

$$\begin{aligned} & \frac{1}{\delta t} (u_{i,h}^{k+1}, v_h) + a_s(u_{i,h}^{k+1}, v_h) + b_s(\mathbf{u}_h^k, u_{i,h}^{k+1}, v_h) \\ & = \frac{1}{\delta t} (u_{i,h}^k, v_h) + (f_i^{k+1}, v_h) - (\partial_i(2p_h^k - p_h^{k-1}), v_h). \end{aligned}$$

After introducing a suitable finite element representation of the variables, the equation above assumes the matrix form

$$\left[\frac{1}{\delta t} \mathbf{M} + \nu \mathbf{K} + \mathbf{B}(\mathbf{U}^k) \right] \mathbf{U}_i^{k+1} = \mathbf{S}_i^{k+1},$$

where \mathbf{M} and \mathbf{K} are the mass and stiffness matrices of a scalar problem, $\mathbf{B}(\mathbf{U})$ denotes the matrix representation of the operator $b_s(\mathbf{u}_h, \cdot, v_h)$ and \mathbf{U}_i is the vector of nodal values of the velocity component $u_{i,h}$. Furthermore, the source term \mathbf{S}_i^{k+1} is defined by

$$\mathbf{S}_i^{k+1} = \frac{1}{\delta t} \mathbf{M} \mathbf{U}_i^k + \mathbf{M} \mathbf{F}_i^{k+1} - \mathbf{G}_i(2\mathbf{P}^k - \mathbf{P}^{k-1}),$$

where \mathbf{G} denotes the matrix of the gradient operator, \mathbf{P} is the vector of nodal values of pressure interpolation, and the remaining symbols have an obvious meaning.

The finite element equation for the incompressible steps reads

$$\hat{\mathbf{K}}(\mathbf{P}^{k+1} - \mathbf{P}^k) = -\frac{1}{\delta t} \hat{\mathbf{D}} \cdot \mathbf{U}^{k+1},$$

where $\hat{\mathbf{K}}$ denotes the stiffness matrix associated with pressure interpolation and $\hat{\mathbf{D}}$ represents the weak form of the divergence operator acting on vector fields interpolated at a higher order than pressure.

6.2. Algorithmic Aspects

The unconditionally stable fractional-step method based on the Poisson equation for pressure described in the previous sections has been implemented using either P_2/P_1 or P_1 -iso- P_2/P_1 finite element triangular meshes. Unstructured Delaunay grids for the two-dimensional test problems have been generated by means of the procedure due to Rebay [26]. This method is simple, efficient, and very convenient for the implementation of adaptive strategies of local refinement.

The integration over the triangles is performed by means of Gaussian quadrature using a three-point formula for the P_1 interpolation and seven-point formula for the P_2 interpolation. This assures the exact evaluation of all scalar products including those which involve the nonlinear convection term. The values of the Jacobian determinant and of the weighting function derivatives at Gauss points of all elements are evaluated once and for all at the beginning of the calculation and stored in arrays for subsequent use.

The algorithm requires us to solve large sparse linear systems of algebraic equations for both the velocity and the pressure. The linear systems for the velocity components are nonsymmetric and change at each time level, while that for the pressure Poisson problem is symmetric and does not depend on time. The solution of these systems is calculated by direct methods using the SPARSPAK library. More precisely, we have used the solution method most suitable for unstructured finite element problems, which minimizes storage requirements by an internal reordering the unknowns obtained by means of the one-way dissection algorithm of George [8]; see also [9, p. 226].

We note that, when Dirichlet conditions are prescribed for velocity on the entire boundary, the matrix of the nonsymmetric linear system in the first step is the same for both velocity components. In this case, it is possible to perform only one (nonsymmetric) factorization per time step, instead of two (resp. three) for problems in two (resp. three) dimensions needed with more general boundary conditions. In any case, at each time step two (three) substi-

tutions are required to determine the velocity in two (three) dimensions and one substitution to determine the pressure.

The Poisson problem for pressure is solved on the pressure mesh using P_1 polynomial interpolation on this mesh. The symmetric matrix of the corresponding equation system is factorized once and for all before the time advancement.

Although all results to be presented in this work were computed using direct solution methods, iterative techniques can also be considered and employed very easily. In particular, in the calculation of accurate transient solutions, which demands rather small values of δt , the factorization of the changing sparse but nonsymmetric matrices for the velocity equations can become too expensive depending of the size of mesh. In these cases, the preconditioned GMRES can be used, possibly in conjunction with an extrapolation for obtaining the initial solution to start the iteration. Such an iterative scheme has been already implemented with success by the authors and appears very promising for simulating three-dimensional flows.

6.3. Convergence Tests

To assess the accuracy of the proposed finite element projection method quantitatively we have conducted convergence tests. For a fixed mesh size h , we have refined the time step and measured the distance between the solution calculated by the projection method and that of the coupled system which is obtained by the iterative solution of the Uzawa operator. The test case concerns the driven cavity, which has been regularized in time by prescribing a top wall velocity depending on time as $U(t) = (t/\tau)^4 / [1 + (t/\tau)^4]$, where $\tau = 0.2$, to fall within the theory of optimal error analysis. We used a uniform triangulation consisting of ≈ 400 P_2 -nodes.

In Fig. 0.1 we plotted the time history ($0 \leq t \leq 1$) of the velocity error for time steps 0.1, 0.05, 0.02, 0.01, 0.005, and 0.002, the norm being the energy norm in $L^2(\Omega)$.

In Fig. 0.2 we plotted the errors of velocity and pressure measured, respectively, by the maximum in time of the energy norm (i.e., $\ell^\infty(0, 1; L^2(\Omega))$) for the velocity (solid line) and by the energy norm in space and time (i.e., $\ell^2(0, 1; L^2(\Omega))$) for the pressure (dotted line). The dashed line corresponds to second-order convergence in time. The striking conclusion of these tests is that the present incremental scheme yields second-order time accuracy, when the error is measured by the distance of the solution from that of the coupled scheme. In a whole, the present scheme is necessarily first-order accurate in time since the solution of the coupled scheme is only first-order accurate. Investigations on the possibility of building (truly) second-order accurate scheme (but only in the L^2 norm) have been carried out by the authors. They will be reported in due time, being far out of the scope of the present work.

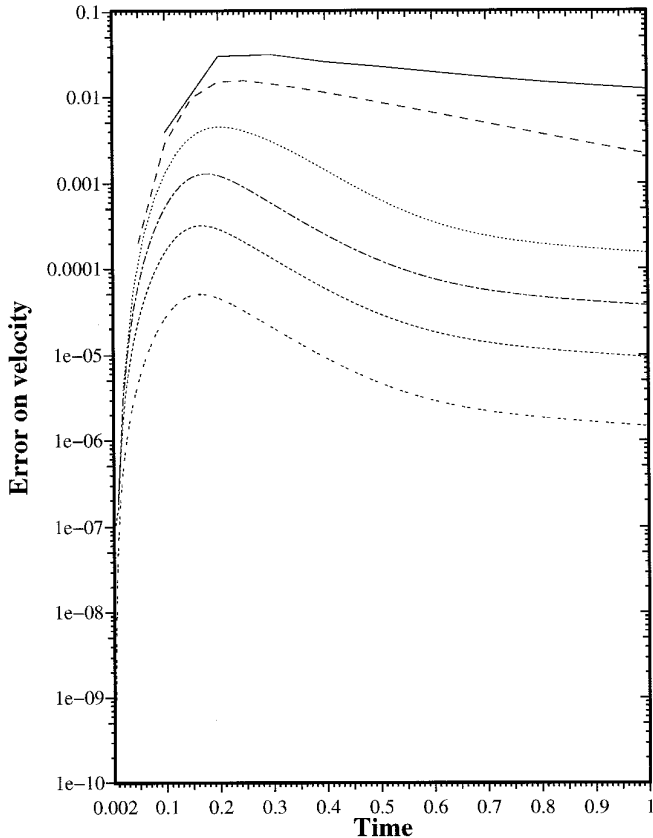


FIG. 0.1. Convergence tests. Time history of the splitting error for $\delta t = 0.1$ (solid line) to $\delta t = 0.002$ (double dashed line).

All these convergence tests confirm also that the projection method (as a splitting technique) retains the optimal space approximation property of the finite elements, while it introduces an error only dependent on the time step, when compared with the unsplit (Uzawa) method.

7. NUMERICAL EXAMPLES AND DISCUSSION

7.1. The Driven Cavity Problem

The first test problem is the driven cavity introduced by Burggraf [3]. The fluid domain is a unit square and the velocity boundary conditions are of zero velocity on the entire boundary except for the upper side of the square where the tangential velocity is equal to 1; the velocity at the corner nodes is fixed to zero to avoid inflow and outflow of the fluid through the first two vertical sides near the corners. The Neumann problem for the pressure is singular and, to have a unique solution the pressure value at the midpoint of the bottom side has been fixed to zero.

The solution for a Reynolds number $R = 100$ has been calculated first on a uniform mesh of 1600 P_2 -nodes. The

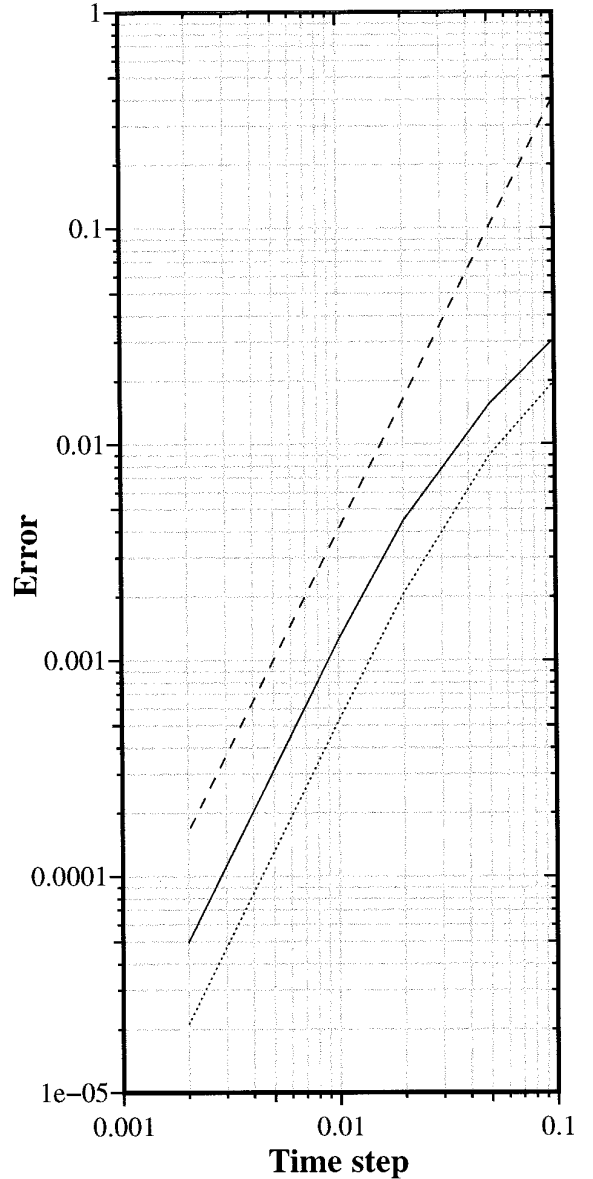


FIG. 0.2. Convergence tests. Splitting error versus time step for the velocity (solid line) and pressure (dotted line); second-order slope (dashed line).

corresponding vorticity ω_h^{k+1} and stream function ψ_h^{k+1} are obtained from the intermediate velocity field \mathbf{u}_h^{k+1} by solving consistent mass matrix problem and a Dirichlet problem, respectively. The solutions are given in Fig. 1.1 and are in a fully satisfactory agreement with the reference solution [10]. We emphasize that in the proposed method the value of the time step has no stability restriction; we verified the numerical stability of the fractional-step algorithm up to $\delta t = 10^3$. Of course, for values of δt not sufficiently small the solution accuracy is completely lost, so

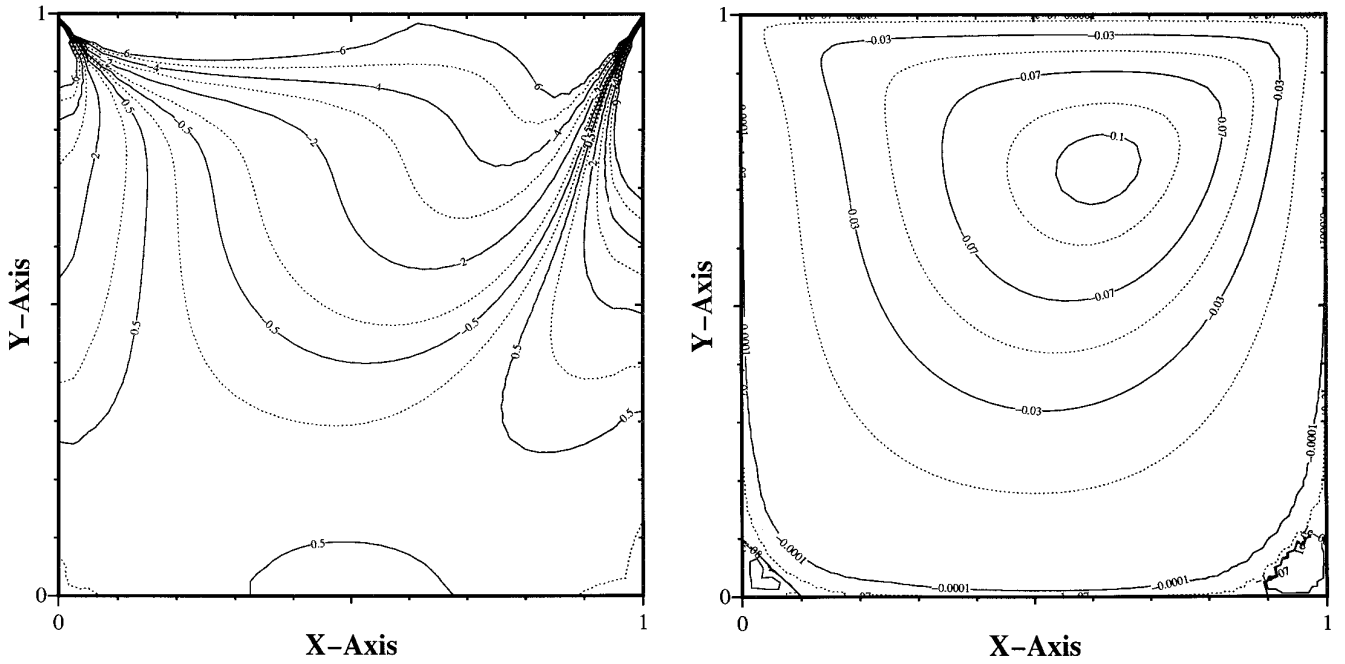


FIG. 1.1. Driven cavity problem with uniform grid of 2×40^2 triangles. Vorticity and streamlines of the steady flow at $R = 100$.

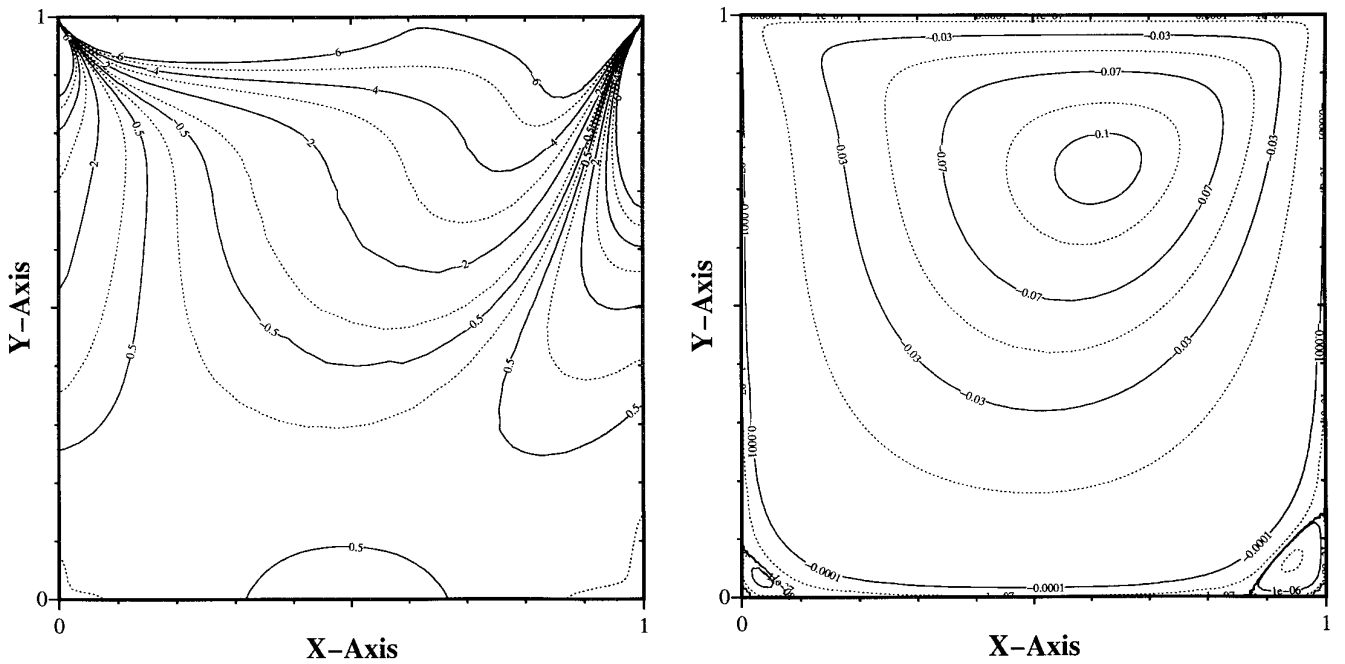


FIG. 1.2. Driven cavity problem with nonuniform grid of ≈ 8800 triangles. Vorticity and streamlines of the steady flow at $R = 100$.

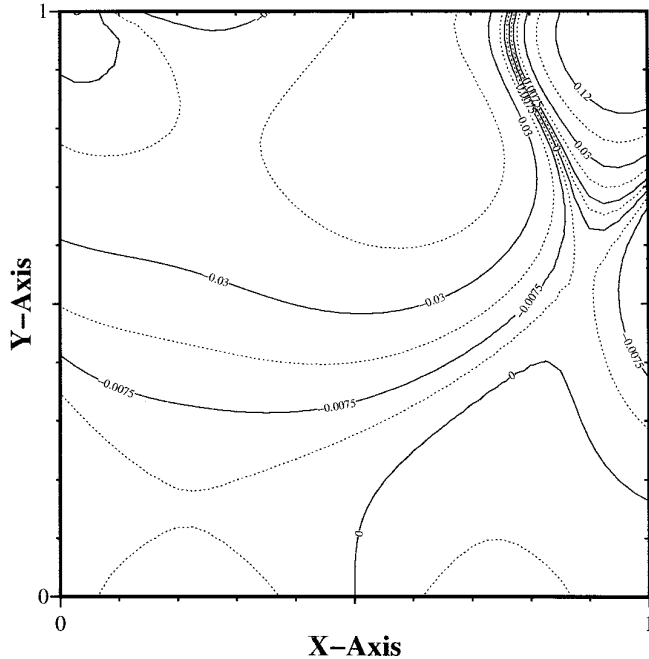


FIG. 1.3. Driven cavity problem. Pressure field of the steady flow at $R = 100$.

the unconditional stability can be helpful to compute steady-state solution or when the advection dynamics is not critical to the answer.

The vorticity field near the corner being sensitive to the size of the considered mesh, we have calculated the solution for $R = 100$ on an unstructured finer mesh with a nonuniform distribution of the triangles near the four corners of the cavity. This mesh consists in a total of ≈ 4500 P_2 -nodes and remains unchanged for higher values of R . The level curves of ω shown in Fig. 1.2 are now very smooth, even in the two corner regions where the vorticity is characterized by a well-known singular behavior.

In Fig. 1.3 the level curves of the pressure field for $R = 100$ calculated are given. The comparison with those provided by the penalty method of the FIDAP program (cf. [20]) is very satisfactory.

The steady solution for $R = 1000$ has been calculated, starting from rest with $\delta t = 0.5$ and reaching a relative difference $|\mathbf{u}_h^{k+1} - \mathbf{u}_h^k|_0 / |\mathbf{u}_h^{k+1}|_0 < 10^{-3}$ in 138 time steps. The plots of the level curves for both ω_h^{k+1} and ψ_h^{k+1} are given in Fig. 1.4. The streamlines are in perfect agreement with those of the reference solution [10]; the same applies for the vorticity contours, except for some wiggles in the central zone of the cavity where the employed mesh is coarsest, while the benchmark solution was calculated on a uniform 129×129 grid.

The steady solutions for $R = 3200$ has been then obtained starting from the $R = 1000$ solution and performing ≈ 100 time steps with $\delta t = 0.1$, and similarly the solution for $R = 5000$. The streamlines of these solutions are given in Fig. 1.5; they compare very well with the reference solutions [10] on uniform 129×129 and 257×257 grids, respectively. All features of the secondary vortices are correctly predicted by the proposed primitive variable method.

We have calculated also the transient solution of the square cavity problem with a sudden start of the sliding top wall at $R = 1000$, using $\delta t = 0.1$. The plots of vorticity and stream function at $t = 5$ calculated by a second-order accurate scheme are shown in Fig. 1.6. The comparison with unsteady solution calculated by a vorticity-stream function formulation given in Fig. 1.7 illustrate the accuracy of the proposed primitive variable method in simulating time-dependent flows.

7.2. Triangular Cavity

The second example is the steady flow in a triangular cavity, investigated numerically very recently [27]. The domain is an equilateral triangle with vertices in $(0, -2a)$ and $(\pm\sqrt{3}a, a)$. The top horizontal wall is sliding with velocity U . We have used a nearly uniform mesh of ≈ 5100 P_2 -nodes; ≈ 300 P_2 -nodes are on the three sides of the triangular domain. The steady solutions for $R = aU/\nu = 100$ and 500 are reported in Figs. 2.1 and 2.2, respectively. The comparison with the solutions calculated by a biharmonic stream function formulation [27] is excellent. All fine details of the latter are faithfully reproduced by the present projection method.

To show the application of boundary conditions different from purely Dirichlet conditions on velocity along the entire boundary, we have also considered a variant of this triangular driven cavity, which is obtained by relaxing the no-slip condition on one of the two fixed sides and imposing on it a slip condition ($\nabla \times \mathbf{u} = 0$), together with the no-penetration condition ($\mathbf{u} \cdot \mathbf{n} = 0$). In the present *uncoupled* implementation of the projection method (cf. Section 5.5), such a pair of boundary conditions can be imposed only on a straight side parallel to a Cartesian axis. Therefore, to solve this boundary value problem the cavity is rotated to put the side with the slip condition in a horizontal position. The sliding wall with the no-slip condition is now inclined with respect to the axes. The corresponding solution for $R = 100$ is given in Fig. 2.3. The flow changes in the region near the slip side can be easily seen (modulo a rotation of $2\pi/3$) by confronting this solution with that shown in Fig. 2.1. Note that in this problem the two systems of equations for the Cartesian components of velocity are different, as a consequence of the kind of boundary conditions.

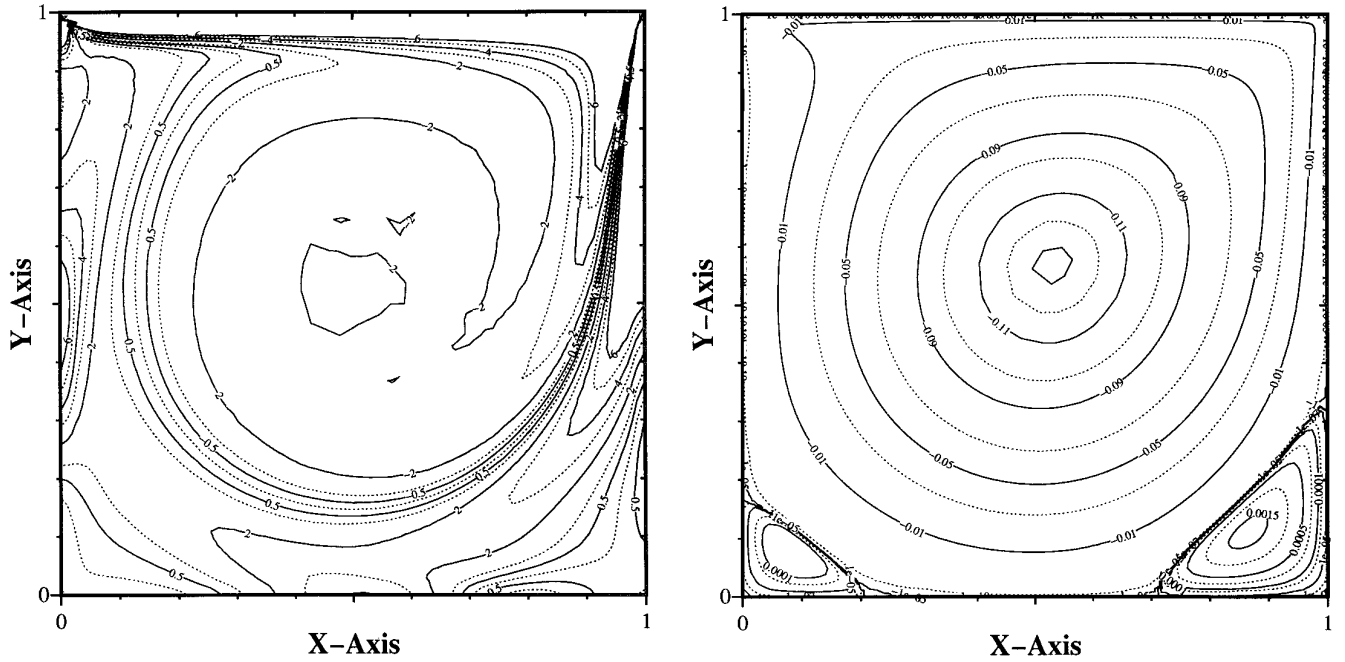


FIG. 14. Driven cavity problem with nonuniform grid of ≈ 8800 triangles. Vorticity and streamlines of the steady flow at $R = 1000$.

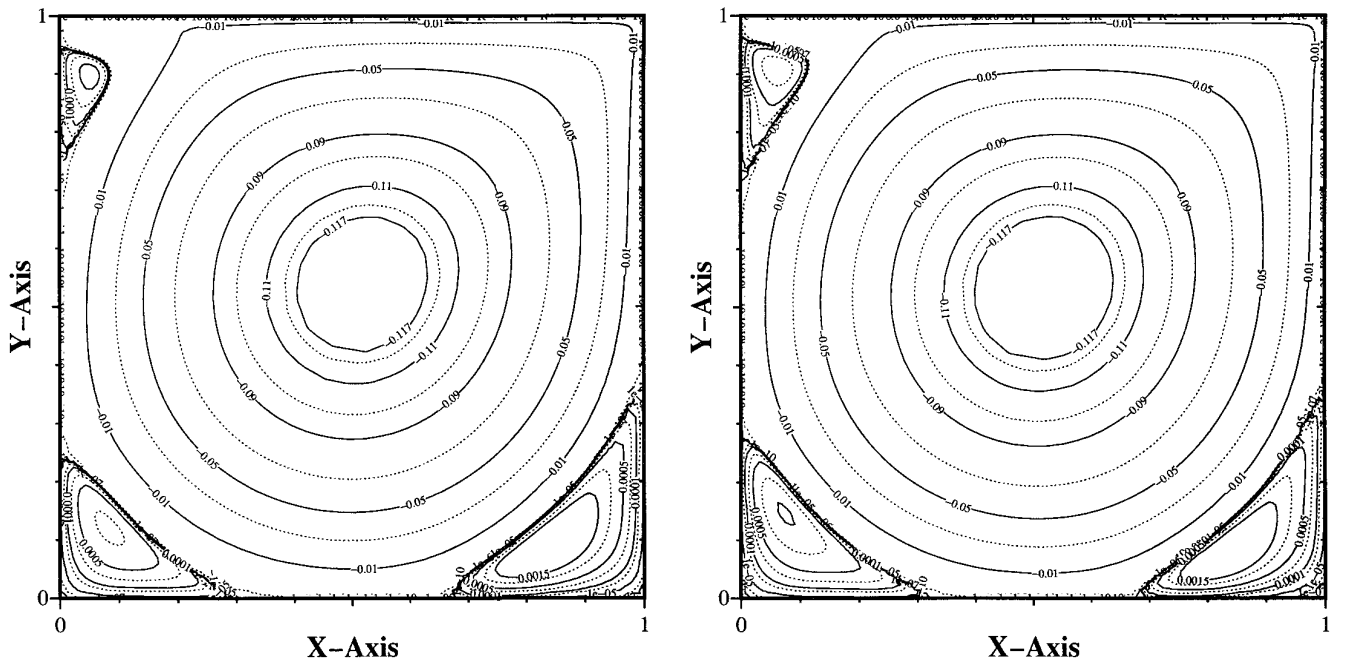


FIG. 15. Driven cavity problem with nonuniform grid of ≈ 8800 triangles. Streamlines of the steady flow at $R = 3200$ (left) and at $R = 5000$ (right).

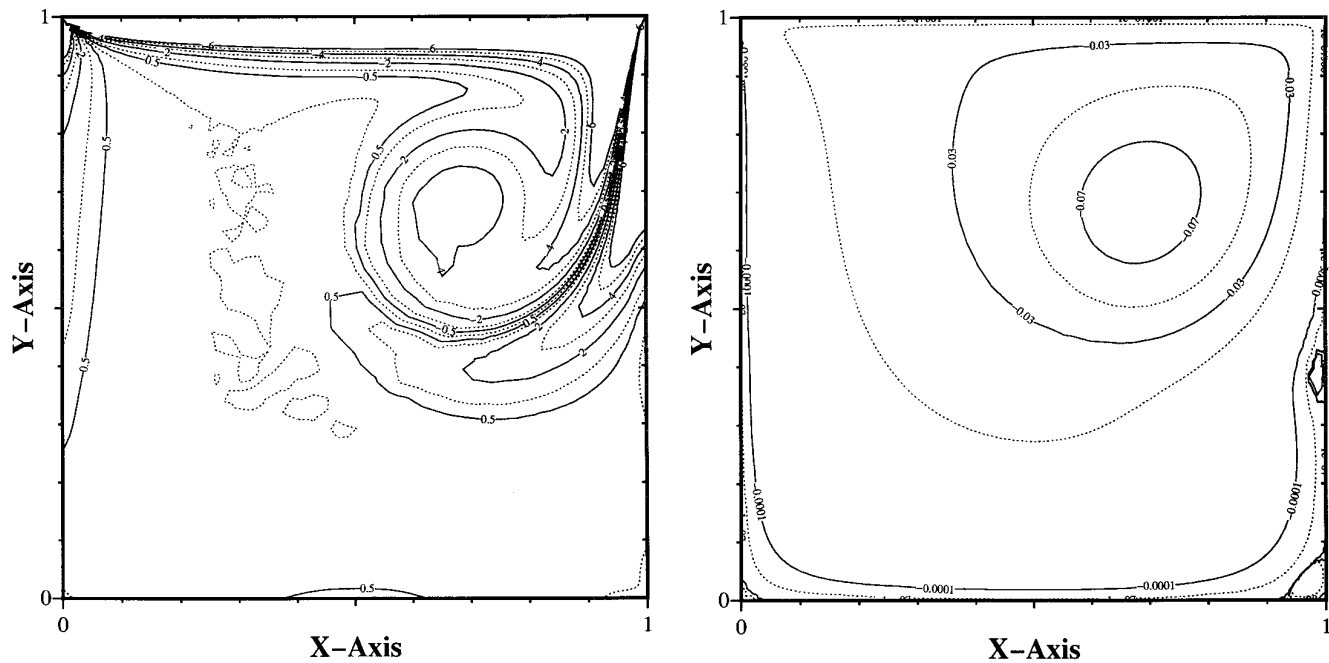


FIG. 16. Unsteady driven cavity problem. Vorticity and streamlines at $t = 5$ for a sudden start with $R = 1000$.

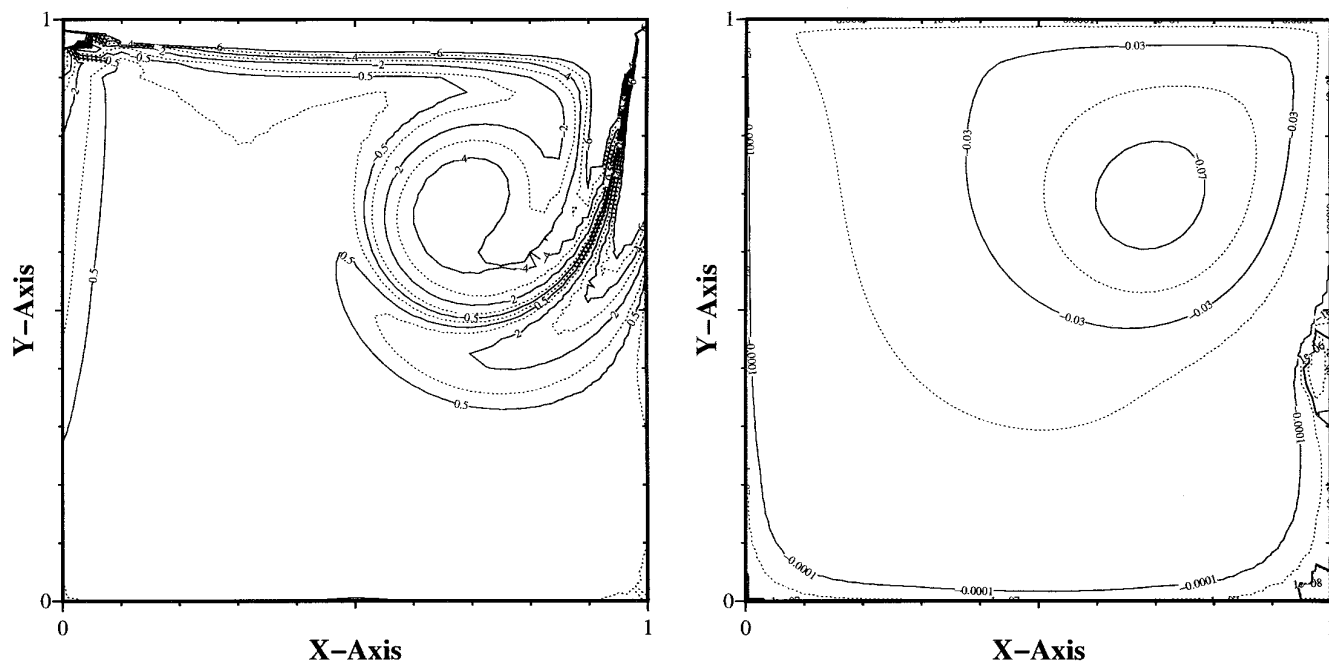


FIG. 17. Unsteady driven cavity problem. Vorticity and streamlines at $t = 5$ for a sudden start with $R = 1000$, obtained by solution of the vorticity/stream function equations.

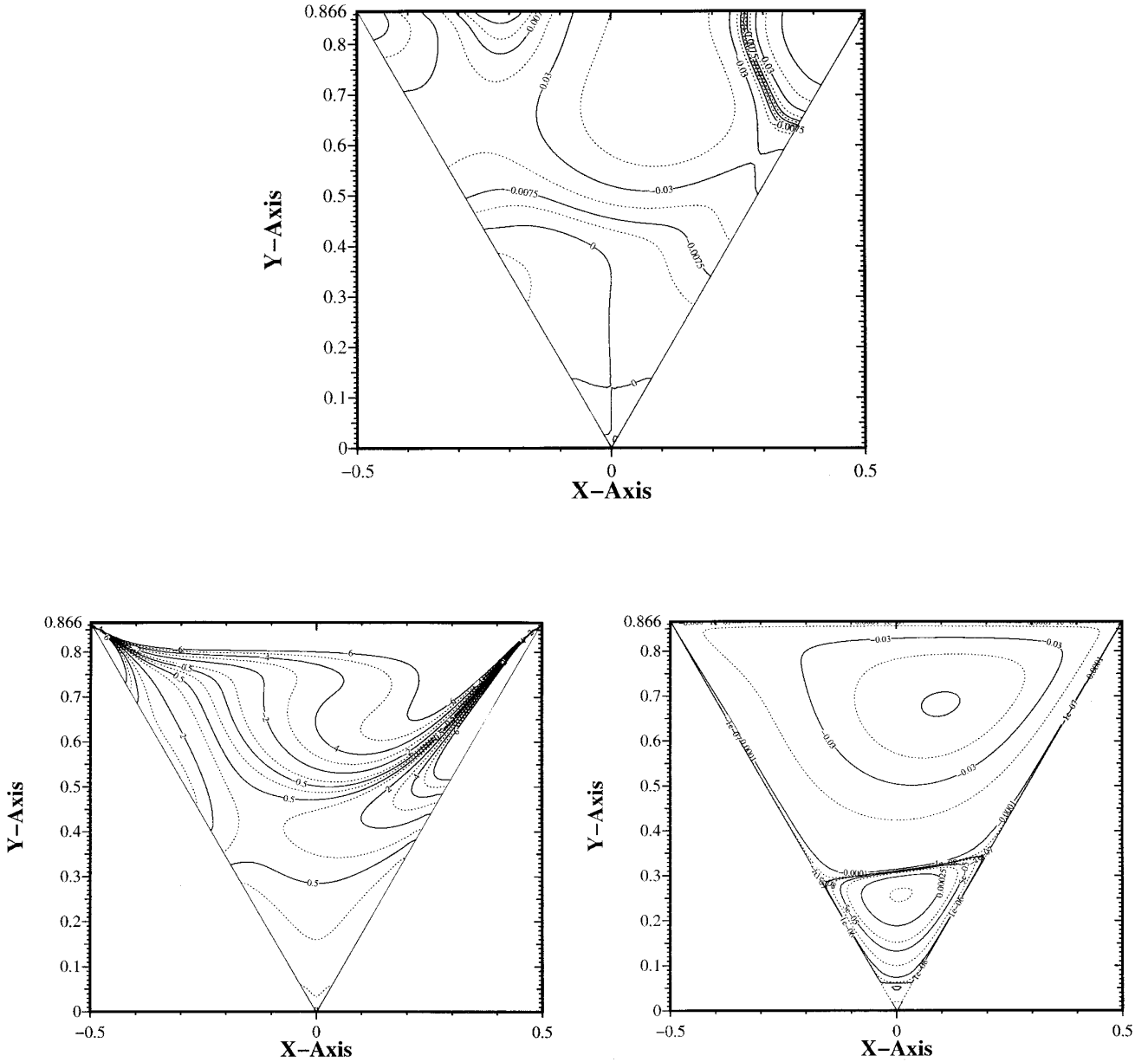


FIG. 2.1. Triangular cavity problem. Pressure (top), vorticity (left), and streamlines (right) of the steady flow at $R = 100$.

7.3 The Backward-Facing Step

The third test problem is the determination of the separated flow in a sudden expansion inside a doubly infinite channel, the so-called backward-facing step. The boundary conditions for such a problem include the Dirichlet velocity

condition at the inlet $u_{\text{in}} = (U(y), 0)$, where $U(y)$ is the Poiseuille profile,

$$U(y) = \frac{-6(y - C)(y - S)}{(C - S)^2},$$

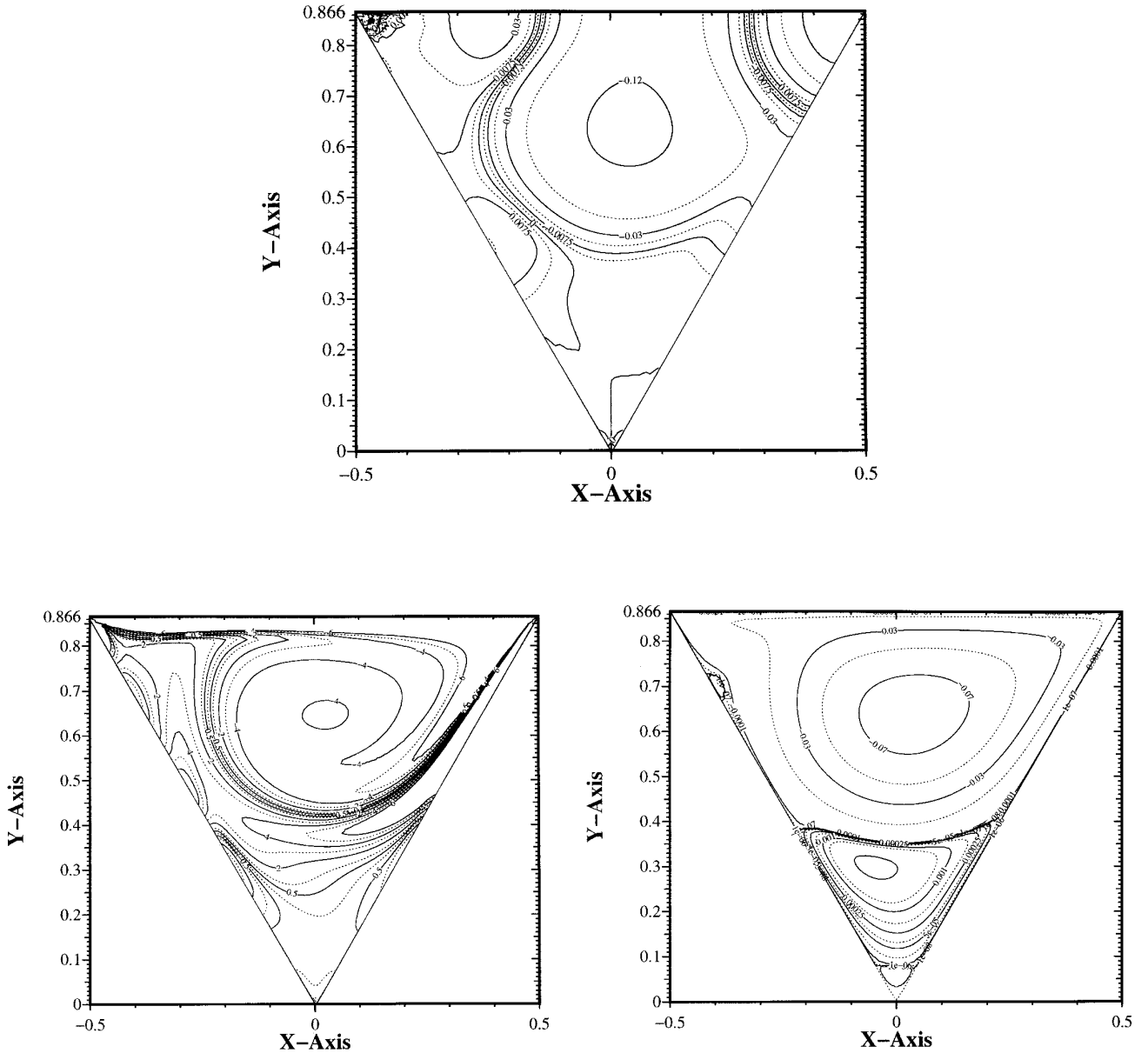


FIG. 2.2. Triangular cavity problem. Pressure (top), vorticity (left), and streamlines (right) of the steady flow at $R = 500$.

C and S being the channel and step height, respectively, and homogeneous velocity conditions on the upper and lower solid walls and on the vertical side of the step. At the outlet the tangential velocity and the pressure are prescribed to be zero. The presence of a boundary condition for pressure means that in the weak form of the momentum equation one has $\mathbf{v} \cdot \mathbf{n}_{\text{out}} \neq 0$. The outlet boundary being

defined by $x = \text{const}$; the weak enforcement of $\nabla \cdot \mathbf{u} = 0$ on it is accounted for only by the equation for the velocity component u_x (in a strong setting the Neumann condition $(\partial u / \partial x)_{\text{out}} = 0$ would be imposed), whereas Dirichlet boundary conditions are imposed on the entire boundary on the component u_y . Therefore, the operators in the equations for the two velocity components are different and

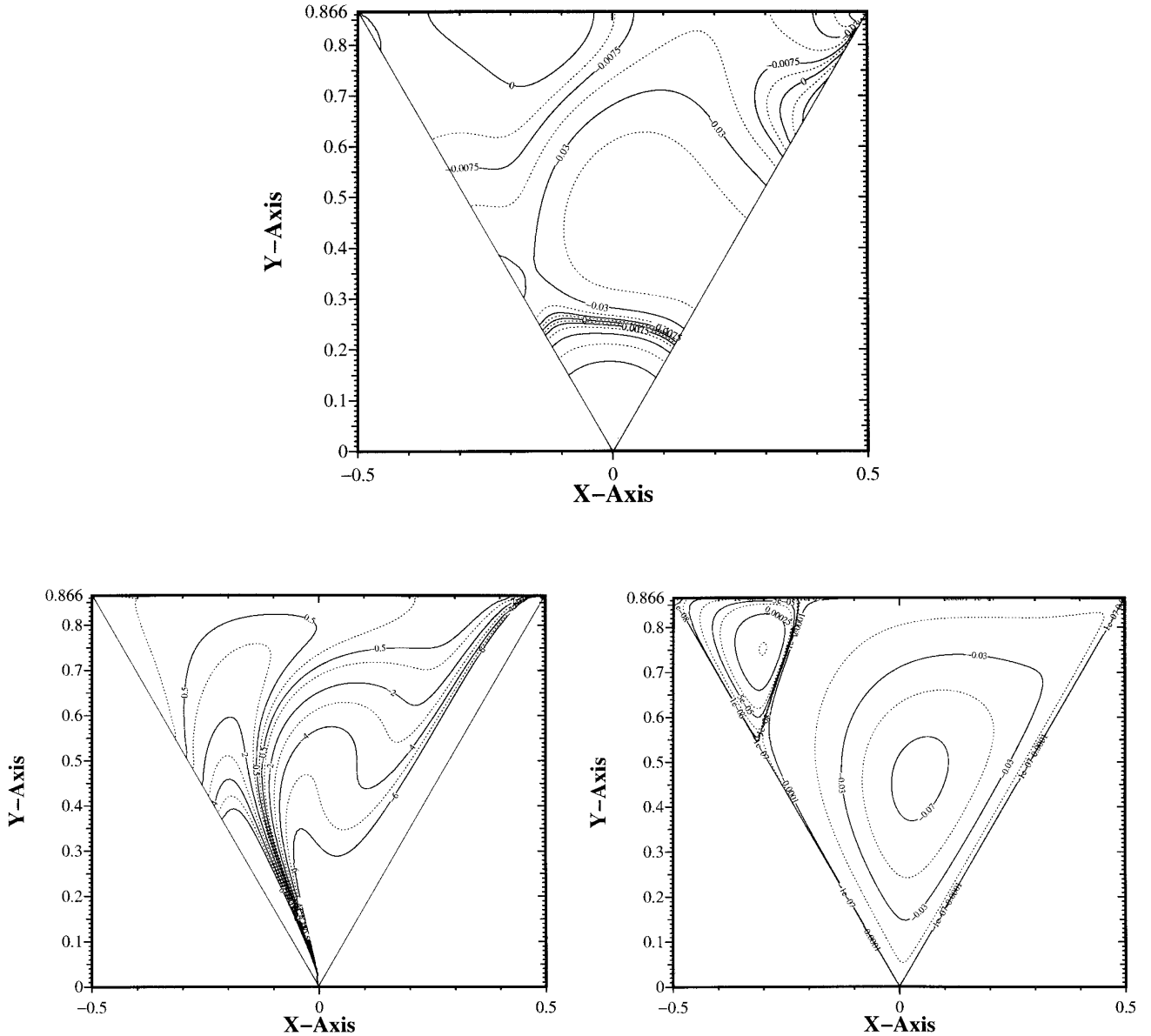


FIG. 2.3. Triangular cavity problem: the top side is fixed and has *slip* boundary conditions. The moving side with no-slip conditions is the left oblique side. Pressure (top), vorticity (left), and streamlines (right) of the steady flow at $R = 100$.

the two equations are uncoupled. As a consequence, the semi-implicit unconditionally stable scheme requires us to build and factorize two different nonsymmetric sparse linear systems at each time step, but the two vector components of the intermediate velocity can be determined independently from each other.

The initial velocity $\mathbf{u}_0(x, y)$ must be chosen so that it is

compatible with the boundary values prescribed on velocity. The compatibility is guaranteed by “prolonging” the inlet Poiseuille velocity profile along the entire length of the channel, by taking

$$\mathbf{u}_0(x, y) = \begin{cases} \mathbf{0} & x > 0, \quad 0 \leq y \leq S, \\ U(y) \hat{\mathbf{x}} & x > 0, \quad S \leq y \leq C. \end{cases}$$

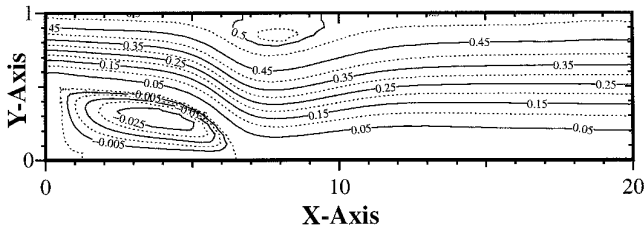


FIG. 3.1. Backward-facing step problem. Streamlines of the steady flow at $R = 800$.

The steady flow in a channel with $C = 1$ and $S = \frac{1}{2}$ has been calculated for $R = 800$ using ≈ 4700 P_2 -nodes distributed nonuniformly over a length $L = 20$. The streamlines of the solution displayed in Fig. 3.1 show two recirculatory regions, one on the lower wall with the reattachment point located at $x = 5.8/C$ downstream from the step, and the other on the upper wall with separation and reattachment points located at $x = 6.1/C$ and $x = 9.0/C$ downstream from the step. These values can be compared with the values 5.93, 4.78, and 10.21, obtained by a pressure correction finite difference method [22]. This discrepancy can be explained, at least partly, by the shorter section of the channel in the present calculation where outflow boundary conditions are imposed and by the lack of refinement of the mesh employed (a systematic comparison of refined solutions is out of the scope of the present paper).

7.4. Unsteady Flow Past NACA 0012 at Incidence

The fourth example is the unsteady flow past a NACA 0012 airfoil with an angle of incidence of 34° and at $R =$

1000. The computational domain is the rectangle $[-2, 5] \times [-3, 3]$, and the airfoil centre is placed at the origin. The boundary conditions for this external problem are:

- zero velocity on the airfoil;
- for $x = -2$: $\mathbf{u} = U\hat{\mathbf{x}}$;
- for $y = \pm 3$: $\mathbf{u} \cdot \mathbf{n} = 0$, $\partial u_\tau / \partial n = 0$, which means $u_y = 0$, $\partial u_x / \partial y = 0$;
- for $x = 5$: $\partial u_x / \partial x = 0$, $u_y = 0$ and $p = 0$.

The mesh for solving the problem with $R = 1000$ consists of ≈ 3600 P_2 -nodes. No attempt has been made to refine the mesh according to the computed solution and we have used a fixed time step $\delta t = 0.02$.

The streamlines at $t = 1.6$ provided by the present projection method are compared in Fig. 4.1 with those calculated by a vorticity stream function method [18]. Figure 4.2 shows the pressure fields at the same time $t = 1.6$ by these two methods. Figures 4.3 and 4.4 contain the streamlines at times $t = 2.8$ and 3.6 , respectively, always compared with those of the ω - ψ solution. Finally, Fig. 4.5 gives the streamlines at the two later times, $t = 4.8$ and 6.0 . The comparison with other solutions at the same times, calculated by a different primitive variable method [6], as well as by a nonprimitive variable method using domain decomposition [28], is fully satisfactory.

7.5. Unsteady Flow Past a Multibody Airfoil

The last example is the determination of the unsteady flow past a multiple-body profile with high-lift devices, consisting of a slat, the main airfoil, and a flap [21]. The angle of incidence is assumed to be 25° .

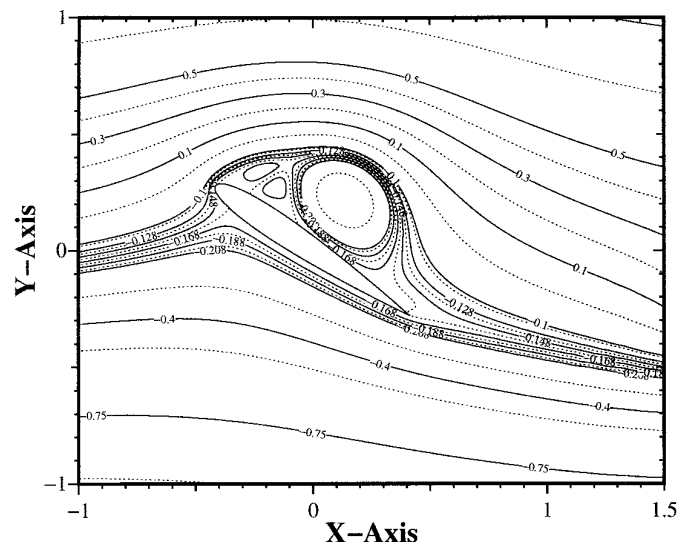
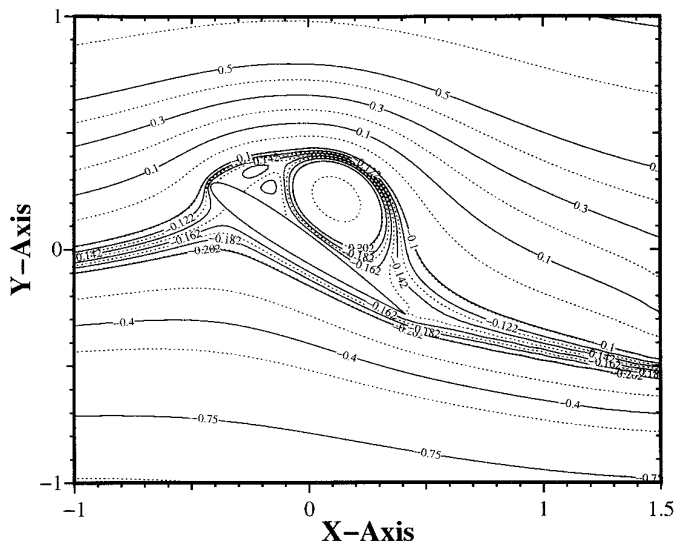


FIG. 4.1. NACA 0012 airfoil at $\alpha = 34^\circ$ and $R = 1000$. Comparison of \mathbf{u} - p (left) and ω - ψ (right) solutions at $t = 1.6$.

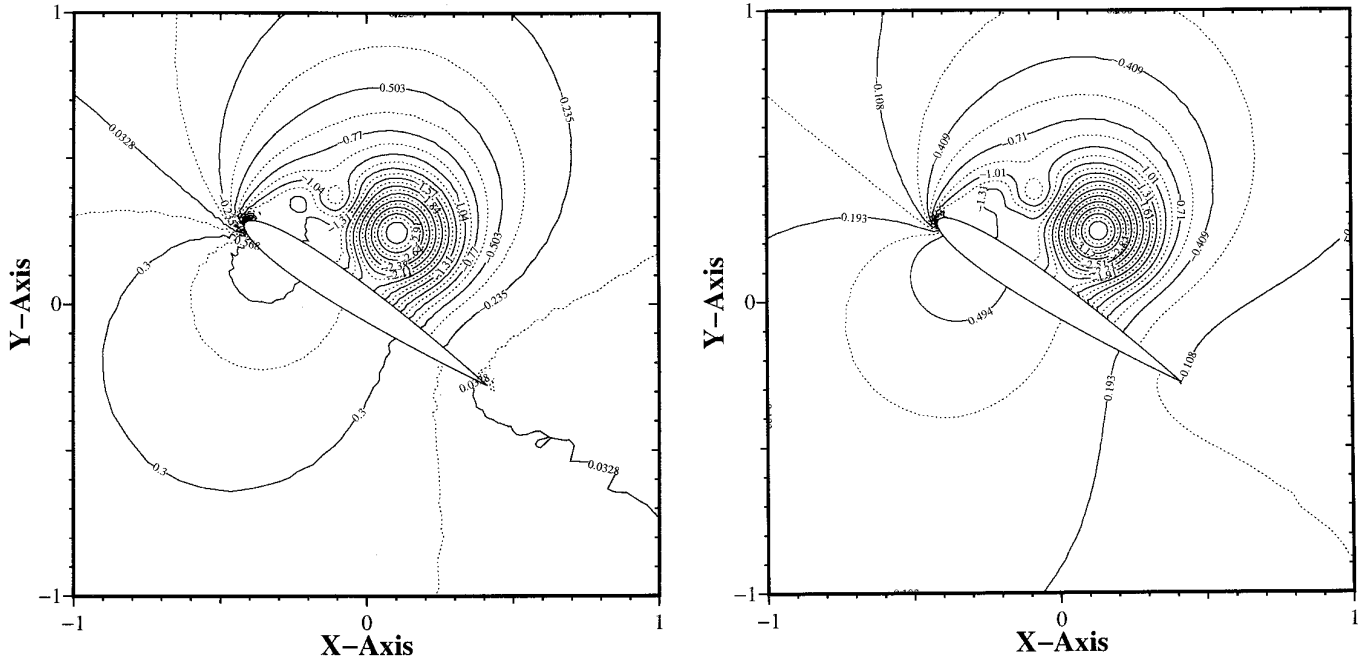


FIG. 4.2. NACA 0012 airfoil at $\alpha = 34^\circ$ and $R = 1000$. Pressure fields of the $u-p$ (left) and $\omega-\psi$ (right) solutions at $t = 1.6$.

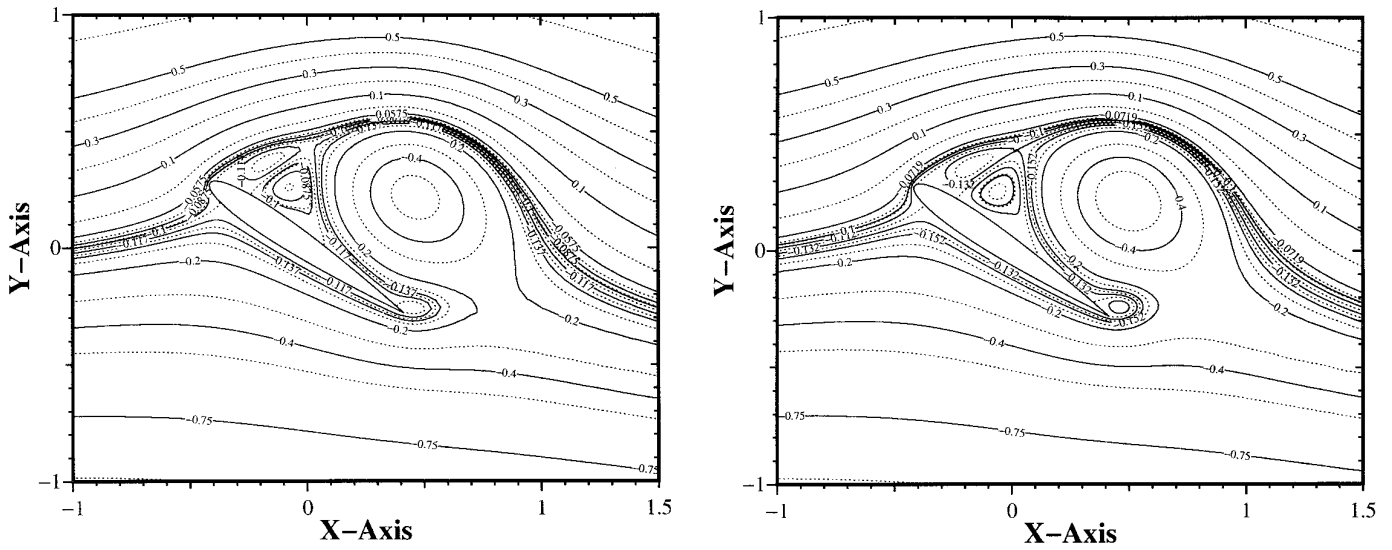


FIG. 4.3. NACA 0012 airfoil at $\alpha = 34^\circ$ and $R = 1000$. Comparison of $u-p$ (left) and $\omega-\psi$ (right) solutions at $t = 2.6$.

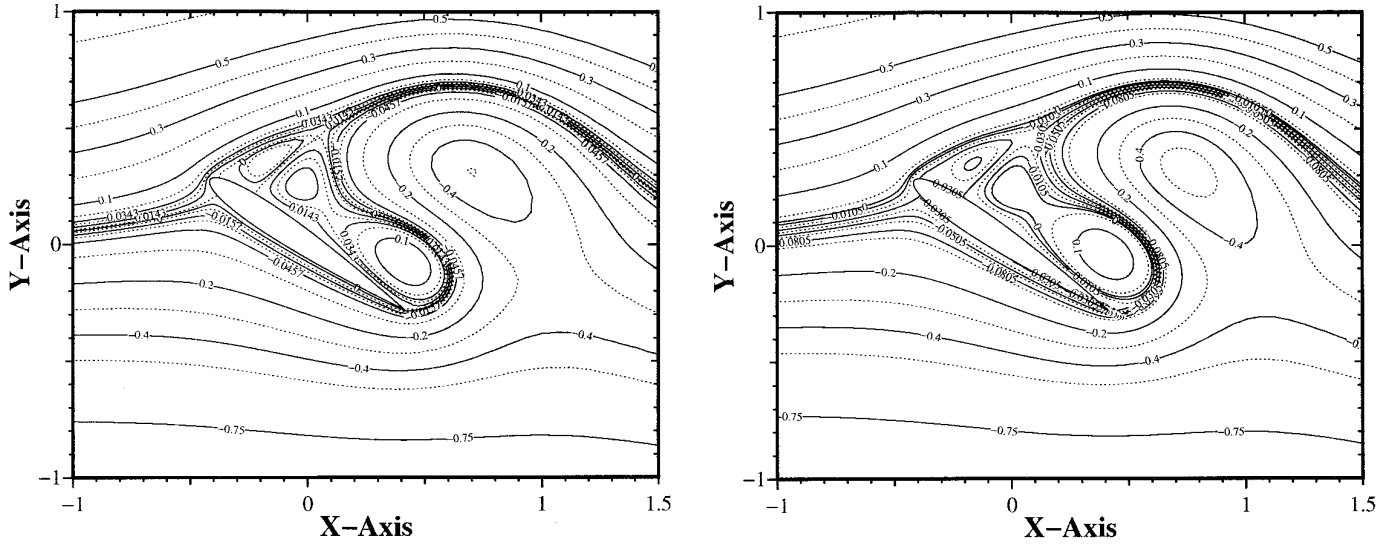


FIG. 4.4. NACA 0012 airfoil at $\alpha = 34^\circ$ and $R = 1000$. Comparison of u - p (left) and ω - ψ (right) solutions at $t = 3.6$.

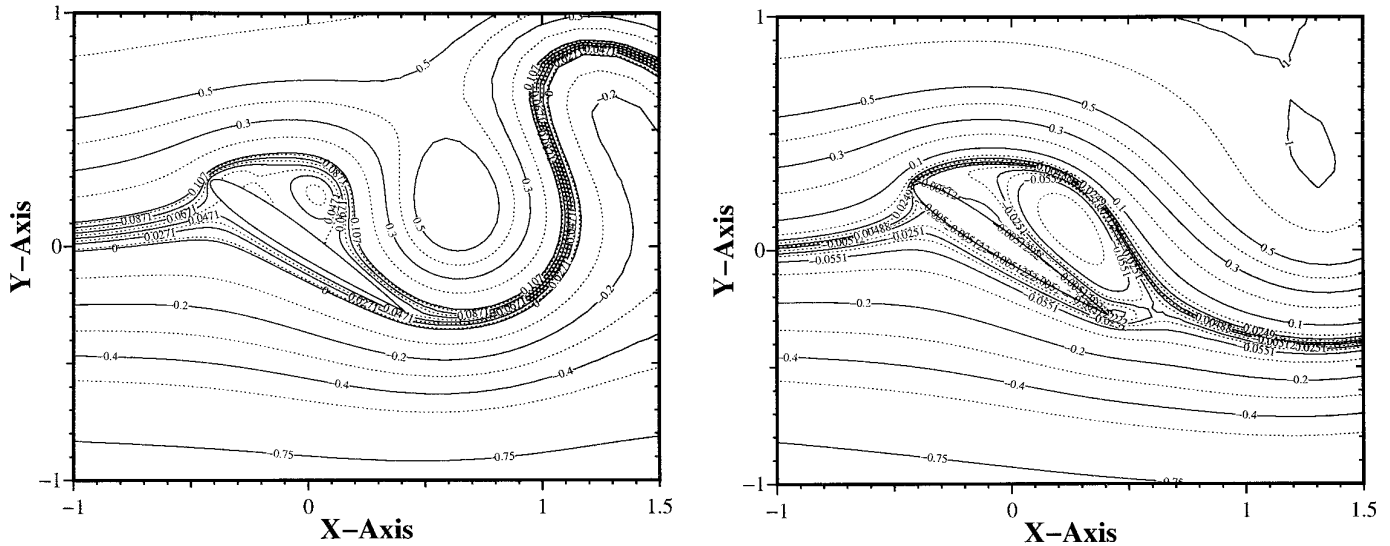


FIG. 4.5. NACA 0012 airfoil at $\alpha = 34^\circ$ and $R = 1000$. Solutions by projection method at $t = 4.8$ (left) and $t = 6.0$ (right).

The computational domain and the boundary conditions are assumed as in the previous external problem. The initial velocity field \mathbf{u}_0 is calculated by solving a pure Neumann problem for the potential Φ_0 of an irrotational velocity field which matches the free stream on the external boundary. Then the velocity components $(u_{0,x}, u_{0,y})$ are determined by solving two consistent mass

matrix problems. The streamlines of this potential flow are given in Fig. 5.1.

We have used a nonuniform mesh of ≈ 5750 P_2 -nodes and a time step $\delta t = 0.02$. In Fig. 5.2 we report the streamlines of the u - p solutions at times $t = 2.8$ and 3.6 for $R = 500$. For comparison, in Fig. 5.3 the streamlines calculated from the solutions of a vorticity/stream function method

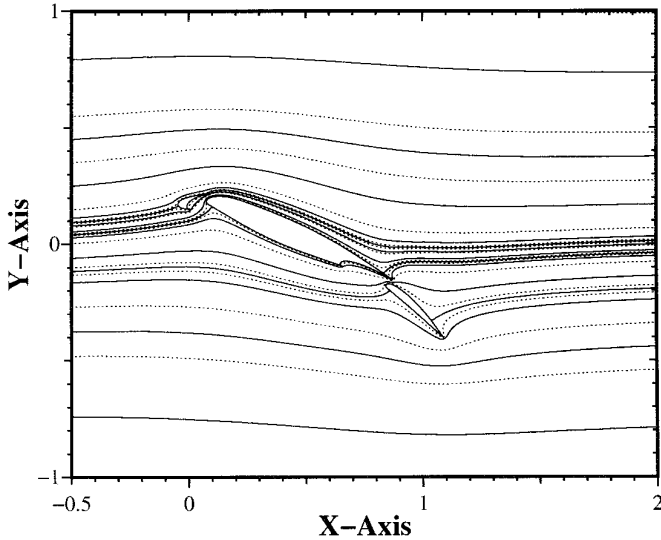


FIG. 5.1. Multibody airfoil at $\alpha = 25^\circ$. Streamlines of the initial potential flow.

[18] at the same times are given. The capability of the present fractional-step projection method to predict unsteady flows in domains of arbitrary shape is therefore demonstrated.

8. CONCLUSIONS

In this paper we have presented a new finite element projection method and its finite element implementation

for unstructured triangular grids using an unconditionally stable integration scheme and a Poisson equation for the pressure increment. A basic aspect of the method is the introduction of *two different* spaces for representing the velocity to be computed in the two (half-) steps of the fractional-step method. In fact, the discrete velocity field provided by the projection step is realized to belong to a space of vector functions which are discontinuous at interelement boundaries. On the other hand, the end-of-step discrete velocity is never explicitly referenced in the numerical algorithm, which is thus formulated only in terms of the intermediate velocity. As a consequence, a computational scheme of utmost simplicity is obtained without sacrificing anything of its functional analytic basis; the final scheme is expressed entirely by Eqs. (5.10)–(5.12).

The comparison of the numerical results provided by the new method with reference solutions is quite satisfactory and the method is found to be capable of predicting internal and external incompressible laminar flows with recirculations and massive separation accurately, without requiring any tuning of the algorithm. In particular, the unconditionally stable semi-implicit treatment of the nonlinear term combined with adaptive mesh generation techniques is expected to be capable of dealing with boundary layers without requiring prohibitively small time steps.

Fractional-step projection techniques are simple to implement, if implemented correctly; in practice we have to solve a succession of convection–diffusion problems and Poisson problems. They are fast; the amount of computation is much lower than that required by coupled techniques such those which are based on the Uzawa operator.

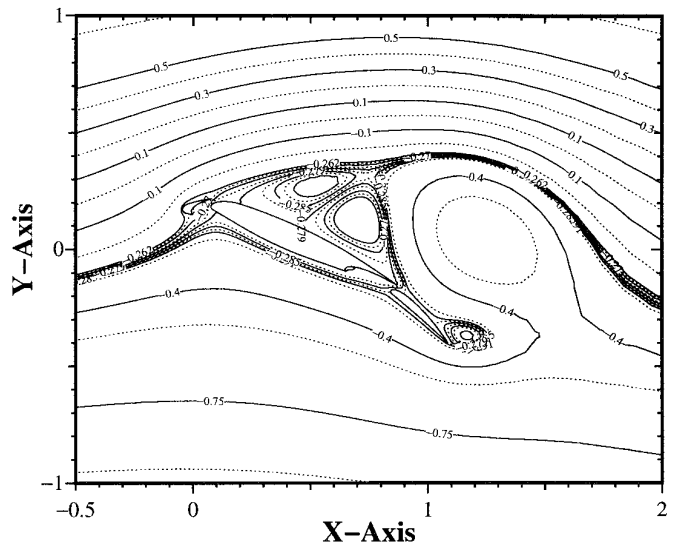
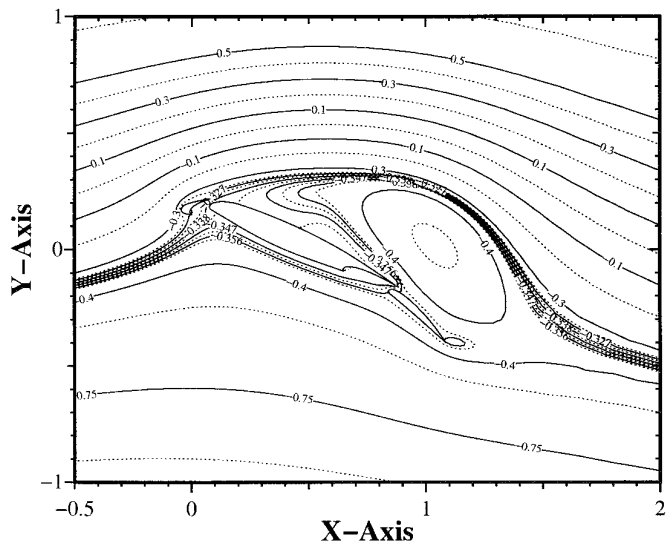


FIG. 5.2. Multibody airfoil at $\alpha = 25^\circ$ and $R = 500$. Solutions of the projection method at $t = 2.8$ (left) and $t = 3.6$ (right).

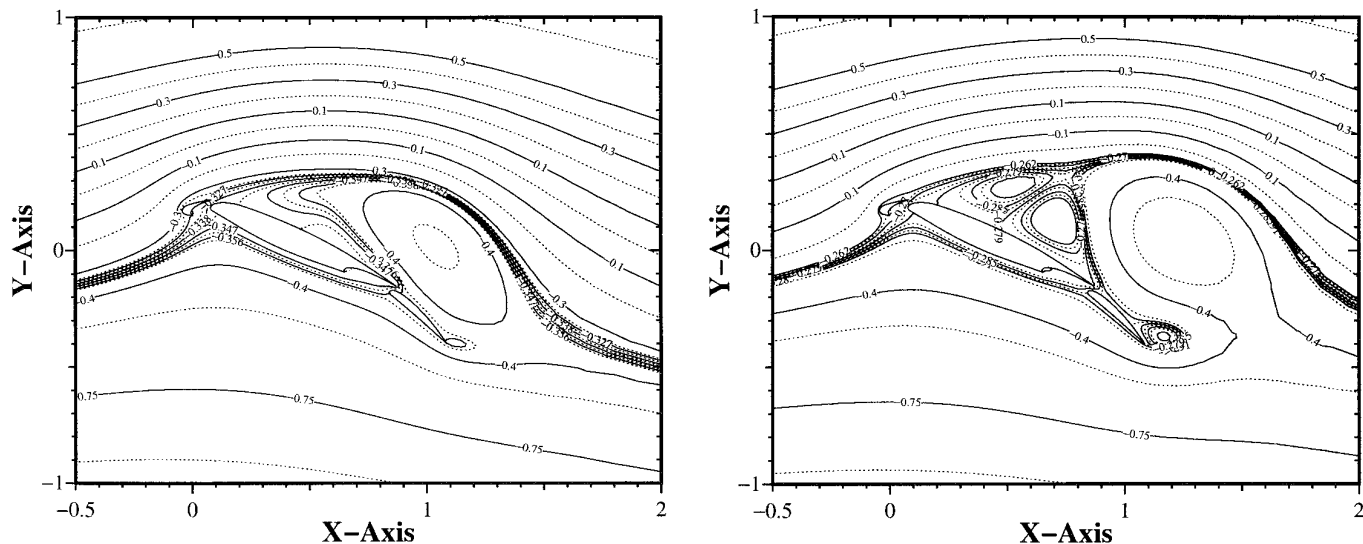


FIG. 5.3. Multibody airfoil at $\alpha = 25^\circ$ and $R = 500$. Solutions of vorticity/stream function equations at $t = 2.8$ (left) and $t = 3.6$ (right).

They yield first-order accuracy in time in the natural norms. If implemented correctly, the projection techniques are very robust—a very desirable feature for industrial applications (see Guermond and Quartapelle [16]). The possibility of second-order accurate projection schemes in the presence of solid no-slip boundaries has not been considered in the present work, but convergence proofs of second-order accuracy in time have been obtained by the authors and will be reported in the near future.

ACKNOWLEDGMENT

The authors are grateful to Alfio Quarteroni for helpful discussions and remarks that improved the content of this paper. The present work has been partly supported by the *Galileo Program*; the support of this program is greatly acknowledged.

REFERENCES

1. C. Bernardi and G. Raugel, *SIAM J. Numer. Anal.* **22**, 455 (1985).
2. F. Brezzi, *RAIRO* **R.2**, 129 (1974).
3. O. R. Burggraf, *J. Fluid Mech.* **24**, 113 (1966).
4. A. J. Chorin, *Math. Comput.* **22**, 745 (1968).
5. A. J. Chorin, *Math. Comput.* **23**, 341 (1969).
6. G. B. Deng, E. Guilmineau, J. Piquet, P. Queutey, and M. Visonneau, *Int. J. Numer. Methods Fluids* **19**, 765 (1994).
7. J. Donea, S. Giuliani, H. Laval, and L. Quartapelle, *Comput. Methods Appl. Mech. Eng.* **30**, 53 (1982).
8. J. A. George, *SIAM J. Numer. Anal.* **17**, 740 (1980).
9. J. A. George and J. W.-H. Liu, *Computer Solution of Large Sparse Positive Definite Systems* (Prentice-Hall, Englewood Cliffs, NJ 1981).
10. U. Ghia, K. N. Ghia, and C. T. Shin, *J. Comput. Phys.* **48**, 387 (1982).
11. V. Girault and P.-A. Raviart, *Finite Element Methods for Navier-Stokes Equations*, Series in Computational Mathematics, Vol. 5 (Springer-Verlag, New York/Berlin, 1986).
12. P. M. Gresho and S. T. Chan, *Int. J. Numer. Methods Fluids* **11**, 587 (1990).
13. J.-L. Guermond, *Modél. Math. Anal. Numér.* **30**, 5 (1996); LIMSI Reports 93-30, 94-07.
14. J.-L. Guermond, *C.R. Acad. Sci. Paris Sér. I* **319**, 887 (1994).
15. J.-L. Guermond and L. Quartapelle, *Int. J. Numer. Methods Fluids* **18**, 471 (1994).
16. J.-L. Guermond and L. Quartapelle, LIMSI Report **95-06**; Unconditionally stable finite-element method for the unsteady Navier-Stokes equations, in *9th International Conference on Finite Elements in Fluids, Venezia, Italy, October 16–20, 1995*, edited by M. Morandi Cecchi *et al.*, p. 367.
17. J.-L. Guermond and L. Quartapelle, On the approximation of the unsteady Navier-Stokes equations by finite element projection methods, submitted.
18. J.-L. Guermond and L. Quartapelle, Uncoupled ω - ψ formulation for plane flows in multiply connected domains, *Math. Mod. Meths. Appl. Sci.* **7**, 6 (1997).
19. J. G. Heywood and R. Rannacher, *SIAM J. Numer. Anal.* **19**, 275 (1982); **23**, 750 (1986); **25**, 489 (1988); **27**, 353 (1990).
20. A. N. F. Mack, *Int. J. Numer. Meth. Fluids* **19**, 795 (1994).
21. I. R. M. Moir, Measurements on a two-dimensional aerofoil with high-lift devices, *Agard Advisory Rep.* **303** (1994).
22. L. Pentaris, K. Nikolados, and S. Tsangaris, *Int. J. Numer. Meth. Fluids* **19**, 1013 (1994).
23. L. Quartapelle, *Numerical Solution of the Incompressible Navier-Stokes Equations* (Birkhäuser, Basel, 1993).
24. A. Quarteroni and A. Valli, *Numerical Approximation of Partial Differential Equations*, Series in Computational Mathematics, Vol. **23** (Springer-Verlag, New York/Berlin, 1994).

25. R. Rannacher, *Lectures Notes in Mathematics*, Vol. **1530** (Springer, Berlin, 1992), p. 167.
26. S. Rebay, *J. Comput. Phys.* **106**, 125 (1993).
27. C. J. Ribbens, L. T. Watson, and C.-Y. Wang, *J. Comput. Phys.*, **112**, 173 (1994).
28. W.-Z. Shen and T-P. Loc, *Int. J. Numer. Methods Fluids* **20**, 1111, (1995).
29. R. Temam, *Navier-Stokes Equations*, Studies in Mathematics and its Applications, Vol. 2 (North-Holland, Amsterdam, 1977).
30. R. Temam, *Bull. Soc. Math. France* **98**, 115 (1968).